Fourier Reconstruction from Non-Uniform Spectral Data

Anne Gelb
School of Mathematical and Statistical Sciences
Arizona State University
anne.gelb@asu.edu

February Fourier Talks
February 17 2011

Research supported in part by National Science Foundation grants
DMS 0510813 and DMS 0652833 (FRG).

MR Imaging Process

- An acquired MR signal can be written as ($2D$ slice)

$$S(k_x, k_y) = \int \int \rho(x, y)\, e^{-i(k_x\, x + k_y\, y)}\, dx\, dy$$

$\rho(x, y)$ is a measure of the concentration of MR relevant nuclei (spins) and

$$k_x = \frac{\gamma}{2\pi} \int_0^t G_x(\tau) d\tau, \quad k_y = \frac{\gamma}{2\pi} \int_0^t G_y(\tau) d\tau$$

  - G_x and G_y are the applied gradient fields
  - We denote the signal acquisition space $\mathbf{k} = (k_x, k_y)$ as "k-space"

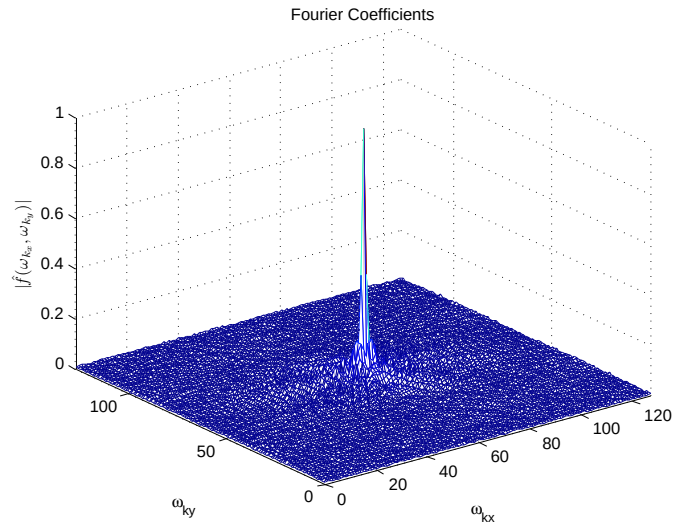

(a) Fourier transform

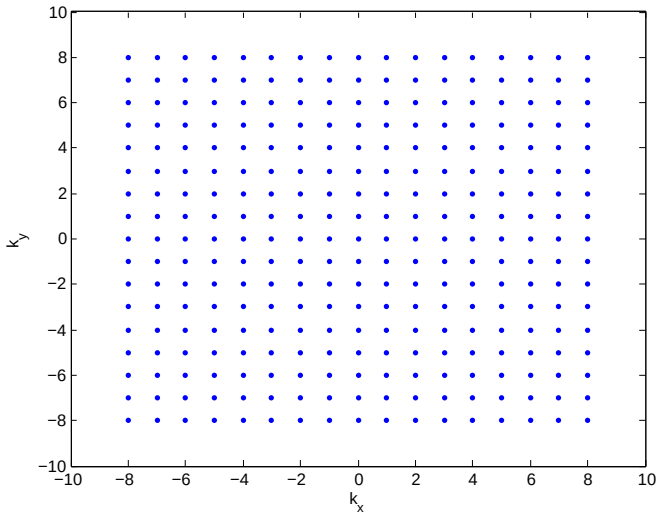

(b) k-space sampling trajectory

Sampling Patterns

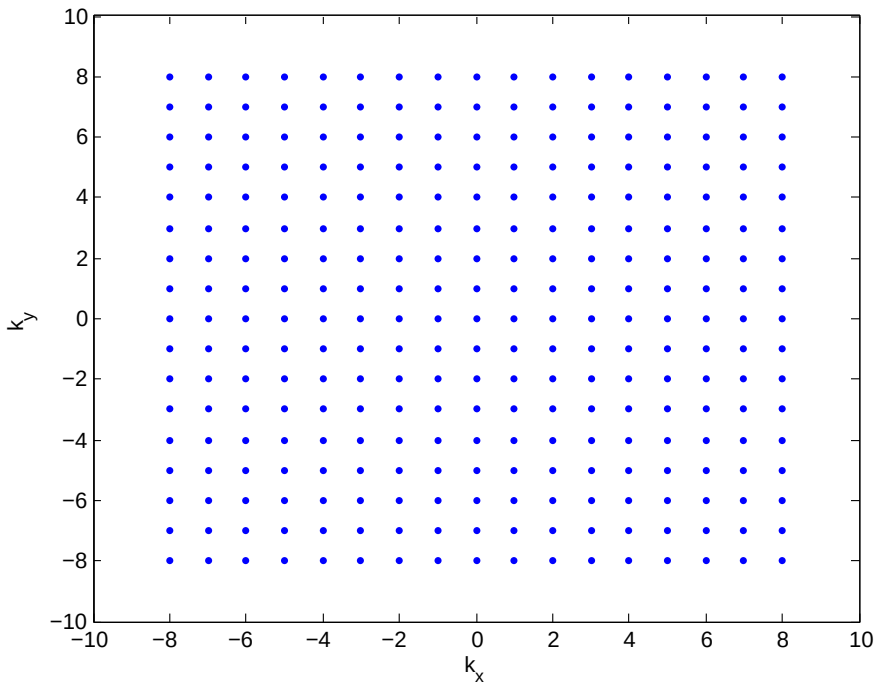

(c) Cartesian Sampling

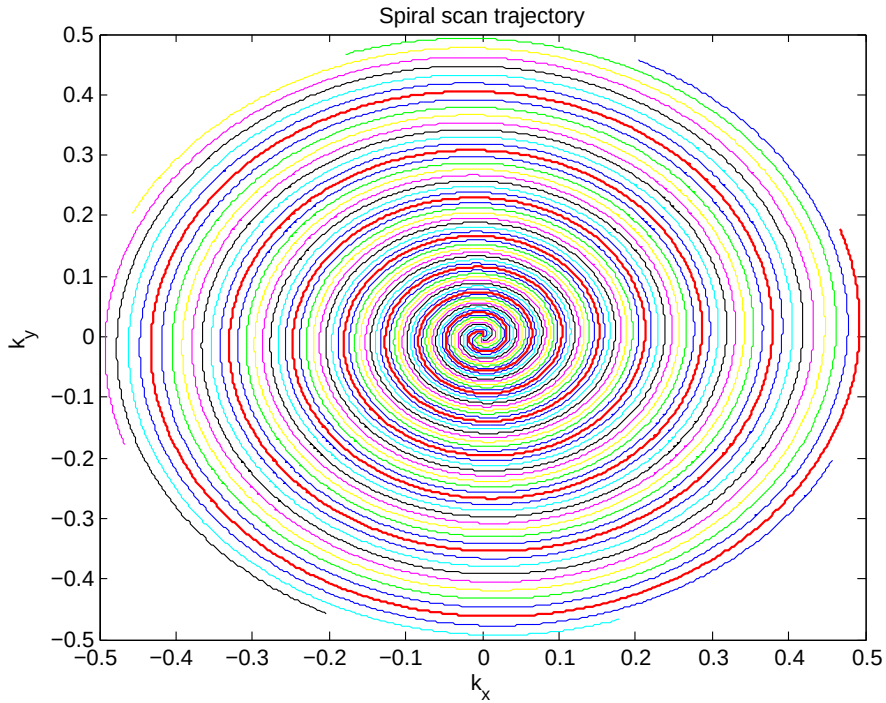

(d) Non-Cartesian Sampling – Spiral Imaging

Figure: MR Imaging Sampling Patterns[1]

[1] Spiral sampling pattern courtesy Dr. Jim Pipe, Barrow Neurological Institute, Phoenix, Arizona

Advantages and Disadvantages of each Pattern

Cartesian Imaging

Advantages

- Well understood and often used in equipment
- Simple reconstruction procedure
- Computationally efficient through use of the standard FFT

Disadvantages

- Susceptible to undersampling – causes aliased images
- Gradient field waveforms can mean sharp transitions in collection

Non-Cartesian Imaging

Advantages

- Less susceptible to aliasing artifacts – aliased images are of "diagnostic quality"
- Easier to generate gradient field waveforms

Disadvantages

- Complex reconstruction procedure (if possible!)
- Computationally demanding – FFT algorithm no longer applies

Advantages and Disadvantages of each Pattern

Cartesian Imaging

Advantages

- Well understood and often used in equipment
- Simple reconstruction procedure
- Computationally efficient through use of the standard FFT

Disadvantages

- Susceptible to undersampling – causes aliased images
- Gradient field waveforms can mean sharp transitions in collection

Non-Cartesian Imaging

Advantages

- Less susceptible to aliasing artifacts – aliased images are of "diagnostic quality"
- Easier to generate gradient field waveforms

Disadvantages

- Complex reconstruction procedure (if possible!)
- Computationally demanding – FFT algorithm no longer applies

Challenges in Cartesian Reconstruction

The Gibbs Phenomenon

- affects the reconstruction of piecewise-smooth functions.
- occurs when data is sampled uniformly or non-uniformly.
- Two important consequences:
  - Gibbs ringing artifact – presence of non-physical oscillations in the vicinity of discontinuities.
  - Reduced rate of convergence to first order even in smooth regions of the reconstruction.
- Why is this important?
  - Oscillations cause post-processing problems in tasks like segmentation, edge detection etc. Filtering oscillations may cause loss of important information.
  - The reduced order of convergence means more Fourier coefficients are needed to obtain a good reconstruction.

The Gibbs Phenomenon – An Example

$$S_N f(x) = \sum_{k=-N}^{N} \hat{f}(k) e^{ikx}, \quad \hat{f}(k) = \frac{1}{2\pi} \int_{-\pi}^{\pi} f(x) e^{-ikx} dx$$

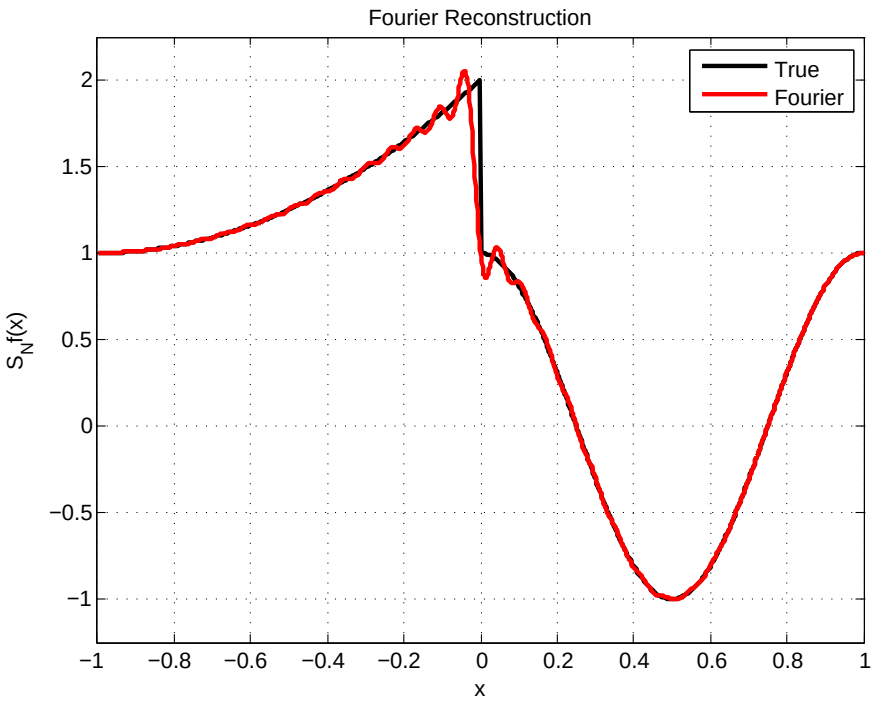

(a) Reconstruction

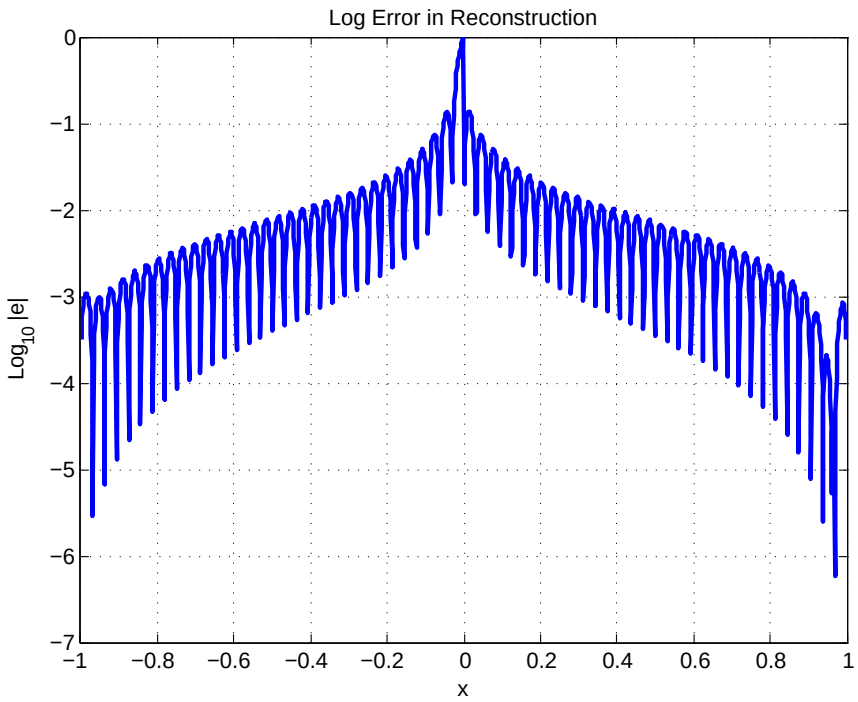

(b) Reconstruction error

Figure: Gibbs Phenomenon, $N = 32$

The Gibbs Phenomenon – An Example

$$S_N f(x) = \sum_{k=-N}^{N} \hat{f}(k) e^{ikx}, \quad \hat{f}(k) = \frac{1}{2\pi} \int_{-\pi}^{\pi} f(x) e^{-ikx} dx$$

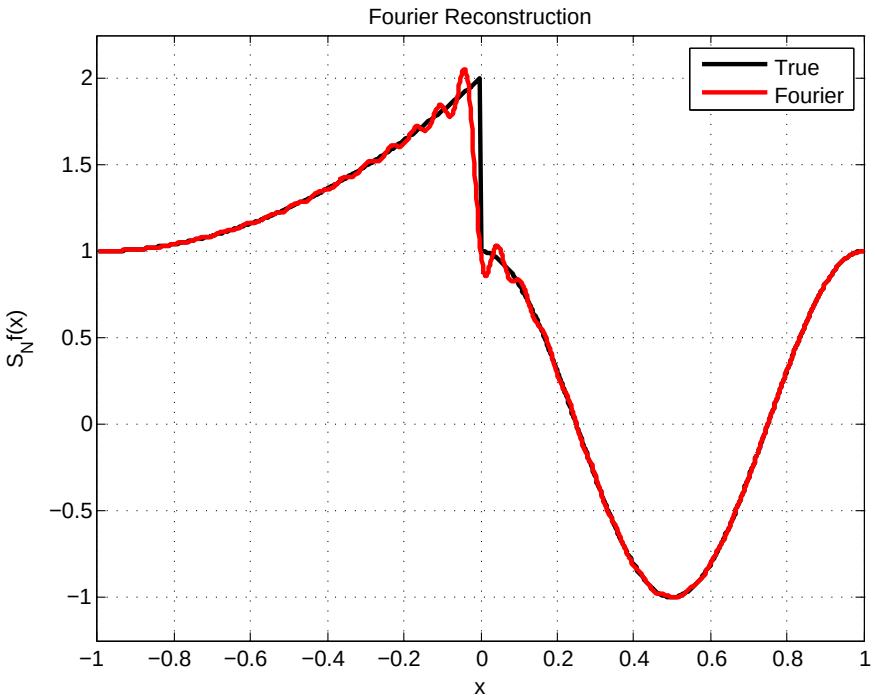

(a) Reconstruction

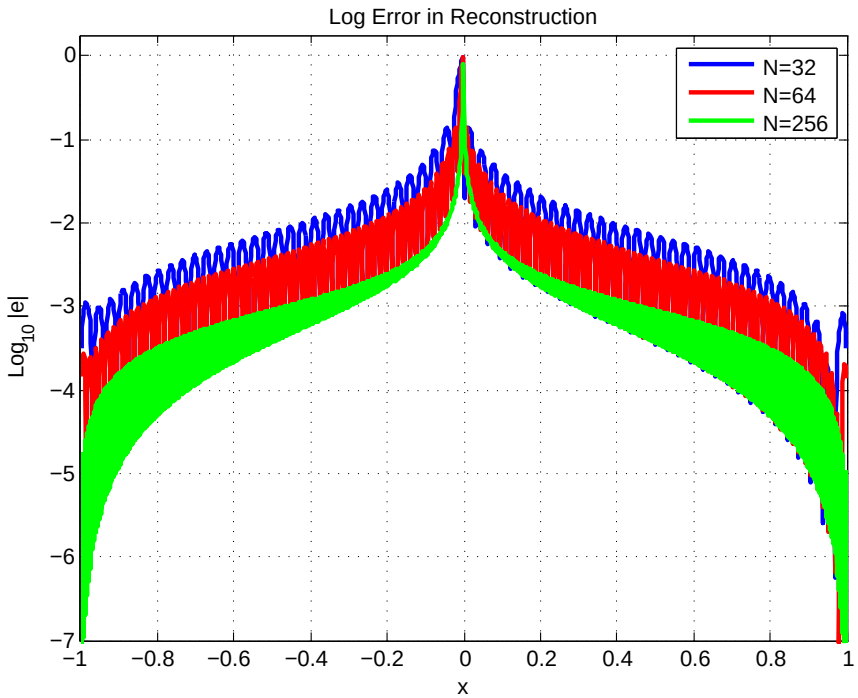

(b) Error does not go away by increasing N

Figure: Gibbs Phenomenon

Shepp Logan MRI

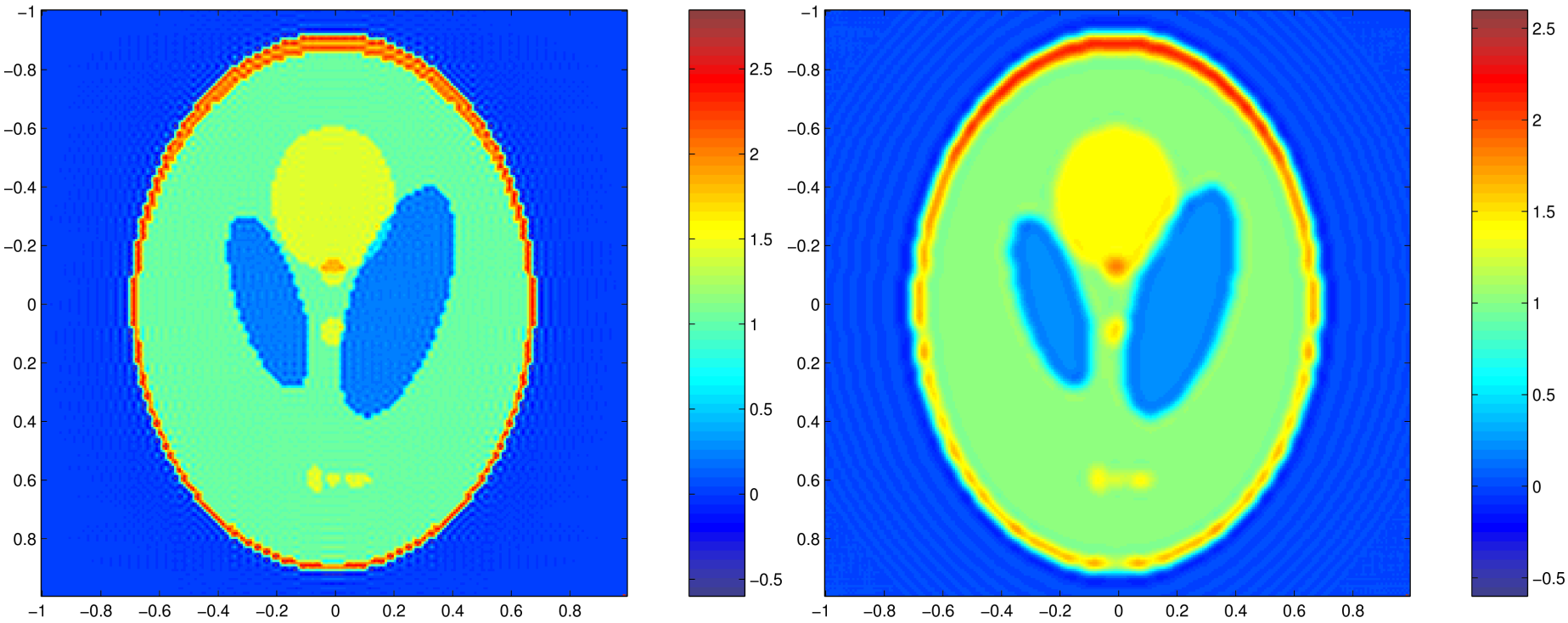

Reconstruction from Fourier Data by Spectral Reprojection (Gottlieb, Shu et. al.)

- Assume that Fourier coefficients $\{\hat{f}_k\}_{k=-N}^{N}$ are given for a piecewise analytic function $f(x)$ in $[-1,1]$
- Use edge detection to determine sub-intervals of smoothness $[a,b]$
- Compute the Fourier partial sum in $[a,b]$: $S_N f(x) = \sum_{k=-N}^{N} \hat{f}_k e^{ik\pi x}$
- Reproject $S_N f(x)$ onto a new basis for $x \in [a,b]$:

$$P_M\big(S_N f(x)\big) \to f(x)$$

- Many other algorithms available (Banerjee & Geer, Driscoll & Fornberg, Eckhoff, Jung & Shizgal, Solomonoff, Tadmor & Tanner, more ...)

Spectral Reprojection (Gottlieb & Shu)

- Goal: approximate a function that is smooth but *not periodic* for $\xi \in [-1, 1]$ (after linear transformation from $x \in [a, b]$)
- We *could* use an orthogonal polynomial expansion,

$$P_M f(x(\xi)) = \sum_{l=0}^{M} a_l \psi_l(\xi), \qquad a_l = \frac{1}{\gamma_l} < f, \psi_l >_\omega$$

but we *have* the Fourier expansion

$$S_N f(x(\xi)) = \sum_{k=-N}^{N} \hat{f}_k e^{ik\pi x(\xi)}$$

- Can we use $S_N f$ to approximate a_l? What should P_M look like?

Spectral Reprojection (Gottlieb & Shu)

- Determine appropriate orthogonal polynomial basis $\{\psi_l(\xi)\}_{l=0}^{M}$ on $[-1,1]$
- Build Fourier approximation inside smooth region $[a,b]$:

$$S_N f(x(\xi)) = \sum_{k=-N}^{N} \hat{f}_k e^{ik\pi x(\xi)}, \qquad x(\xi) = \epsilon\xi + \delta$$

- Expansion coefficients for $\psi_l(\xi)$ are approximated by $b_l = \frac{1}{\gamma_l} < S_n f, \psi_l >_\omega \approx a_l$
- Reprojection in smooth region $[a,b]$:

$$P_m(S_N f(x(\xi))) = \sum_{l=0}^{m} b_l \psi_l(\xi)$$

Spectral Reprojection (Gottlieb & Shu)

Definition: A **Gibbs Complementary Reprojection Basis**, $\{\psi_l\}_{l=0}^{N}$, has the properties:

1. For an analytic function on $[-1, 1]$, the function's expansion in the orthogonal reprojection basis is exponentially convergent, $P_m f(x) \to f(x)$ exponentially for smooth $f(x)$.
2. The projection of the high modes in the original basis on the low modes in the new basis is exponentially small.

If these conditions are met, then

$$P_m(S_N f(x(\xi))) \to f(x) \quad \text{exponentially for } x \in [a, b]$$

Error Analysis For Spectral Reprojection

$$\begin{aligned} Err(m, N, f, \omega) &:= ||f - P_m(S_N f)|| \leq ||f - P_m f|| + ||P_m(f - S_N f)|| \\ &= Trunc(m, f, \omega) + Proj(m, N, f, \omega) \end{aligned}$$

- $Trunc(m, f, \omega)$ measures the convergence properties of the reprojection basis for m expansion coefficients (reflects first Gibbs complementary basis property)
  - Converges exponentially for $\omega(x) \geq 0$
  - $m = \beta N$ expansion terms, $0 < \beta < 1$, resolves the function
- $Proj(m, N, f, \omega)$ measures the near orthogonality of the reprojection space P_m and the space containing the information about the function that is not known, $I - S_N$ (reflects second Gibbs complementary basis property)

Error Analysis For Spectral Reprojection

$$\begin{aligned} Err(m, N, f, \omega) &:= ||f - P_m(S_N f)|| \leq ||f - P_m f|| + ||P_m(f - S_N f)|| \\ &= Trunc(m, f, \omega) + Proj(m, N, f, \omega) \end{aligned}$$

- $Trunc(m, f, \omega)$ measures the convergence properties of the reprojection basis for m expansion coefficients (reflects first Gibbs complementary basis property)
  - Converges exponentially for $\omega(x) \geq 0$
  - $m = \beta N$ expansion terms, $0 < \beta < 1$, resolves the function
- $Proj(m, N, f, \omega)$ measures the near orthogonality of the reprojection space P_m and the space containing the information about the function that is not known, $I - S_N$ (reflects second Gibbs complementary basis property)

Error Analysis For Spectral Reprojection

$$\begin{aligned} Err(m, N, f, \omega) &:= ||f - P_m(S_N f)|| \leq ||f - P_m f|| + ||P_m(f - S_N f)|| \\ &= Trunc(m, f, \omega) + Proj(m, N, f, \omega) \end{aligned}$$

- $Trunc(m, f, \omega)$ measures the convergence properties of the reprojection basis for m expansion coefficients (reflects first Gibbs complementary basis property)
  - Converges exponentially for $\omega(x) \geq 0$
  - $m = \beta N$ expansion terms, $0 < \beta < 1$, resolves the function
- $Proj(m, N, f, \omega)$ measures the near orthogonality of the reprojection space P_m and the space containing the information about the function that is not known, $I - S_N$ (reflects second Gibbs complementary basis property)

Look at Projection Error

The projection error corresponds to the decay rate of the coefficients b_l:

$$\begin{aligned} Proj(m,N,f,\omega) &= P_m(f - S_N f) \\ &= \sum_{l=0}^{m} \psi_l(\xi) \frac{1}{\gamma_l} \langle f - S_N f, \psi_l \rangle_\omega \\ &= \sum_{l=0}^{m} \psi_l(\xi) \frac{1}{\gamma_l} \int_{-1}^{1} \omega(y)\psi_l(y)(f(x(y)) - S_N f(x(y)))dy \\ &= \sum_{l=0}^{m} \frac{1}{\gamma_l} \sum_{|k|>N} \hat{f}_k \psi_l(\xi) \int_{-1}^{1} e^{i\pi k x(y)} \omega(y)\psi_l(y)dy \end{aligned}$$

• Error will be small if the weight function ω is chosen so that the corresponding integral is very small.

Reprojection using the Gegenbauer polynomial basis (Gottlieb, Shu, et. al)

- Define the weight function ω as: $\omega_\lambda(\xi) = (1-\xi^2)^{\lambda-\frac{1}{2}}$. Large λ ensures that $\int_{-1}^{1} e^{i\pi k x(y)}\omega(y)\psi_l(y)dy$ is small. Subsequently, the errors from the boundaries do not enter the approximation
- Corresponding reprojection basis are the Gegenbauer polynomials, $C_l^\lambda(\xi)$.
- Note that Chebyshev ($\lambda = 0$) and Legendre ($\lambda = \frac{1}{2}$) do not make good reprojection bases.

Gegenbauer Reconstruction

- If $\lambda = \lambda(N)$ then the reprojection coefficients

$$b_l := \frac{1}{\gamma_l} \int_{-1}^{1} S_N f(x(\xi)) \psi_l(\xi) (1-\xi^2)^{\lambda(N)-\frac{1}{2}} d\xi,$$

  decay *exponentially*.
- Can rewrite implementation to avoid quadrature (use FFT)
- For many imaging applications, small m and λ work well
- Robust with respect to noise in imaging data (Archibald & Gelb)

Shepp Logan Phantom (Archibald & Gelb)

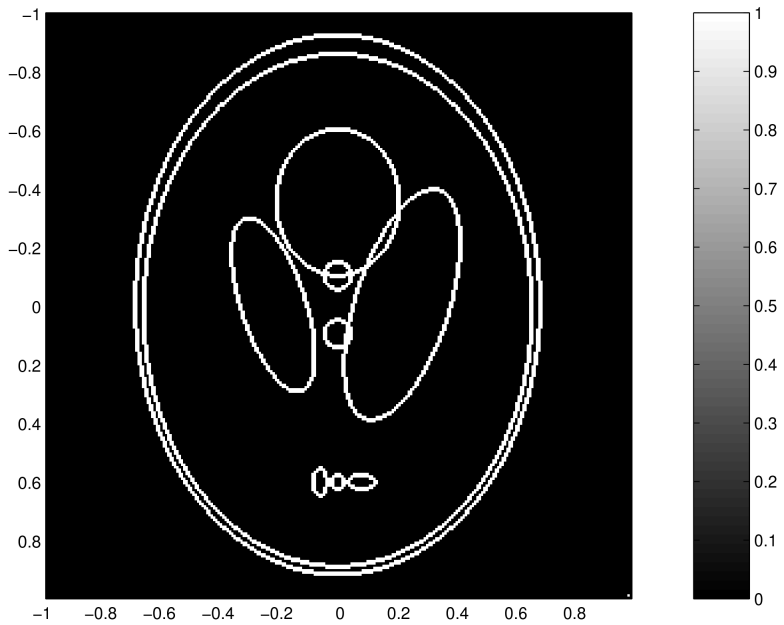

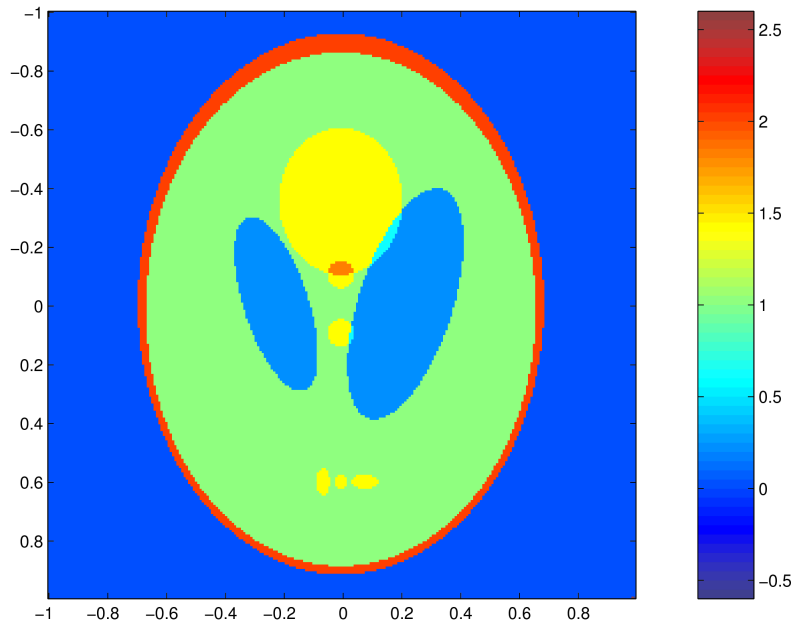

Improvement of image quality for segmentation (Archibald, Chen, Gelb & Renaut)

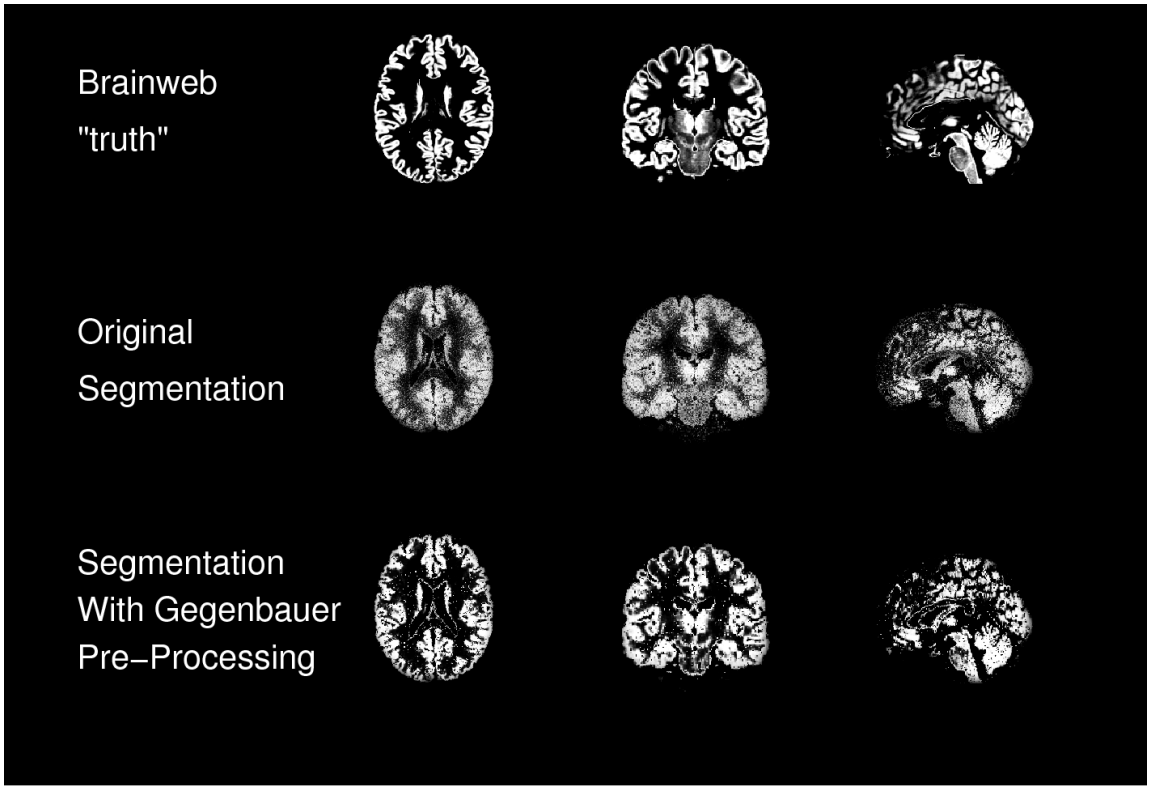

Gray matter segmented probability maps

- 256×256 randomly generated MNI digital brain
- 9% noise level
- non-uniform tissue intensity

Outline

Problem Formulation

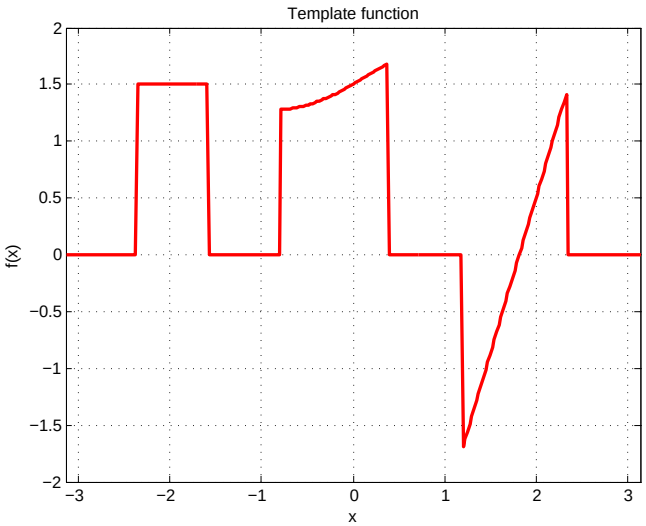

(a) Template Function

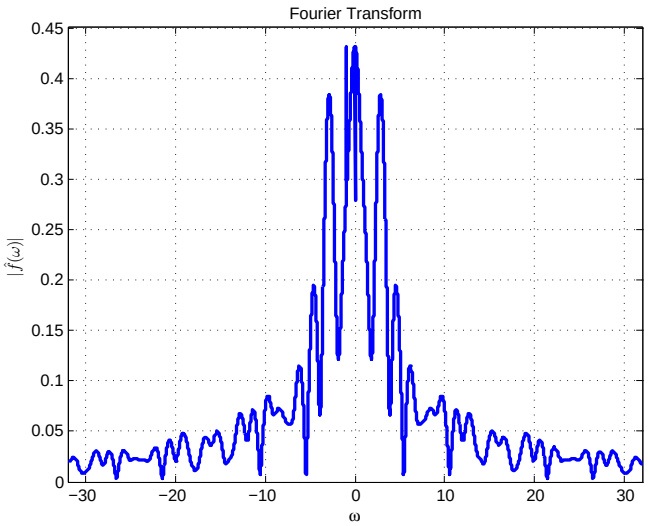

(b) Fourier Transform

- Given these coefficients, can we/how do we reconstruct the function?
- What accuracy can we achieve given a finite (usually small) number of coefficients?
- Computational issue – no FFT available

Problem Formulation

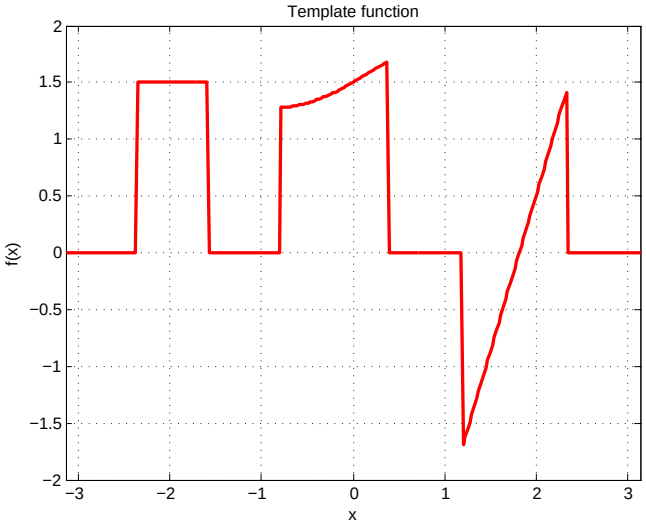

(c) Template Function

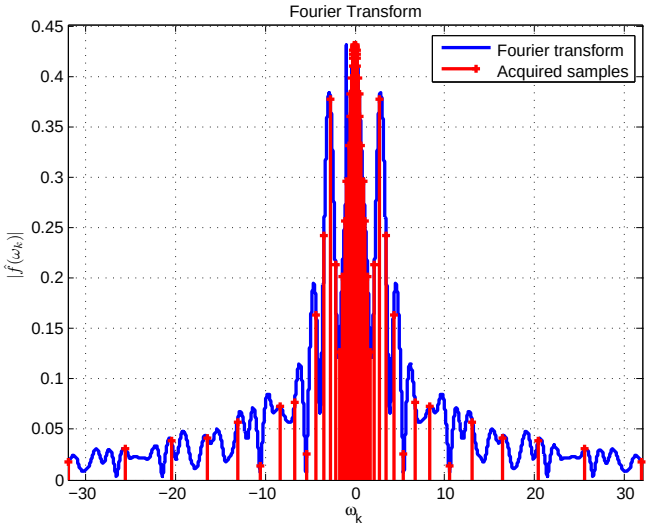

(d) Fourier Coefficients, $N = 32$

- Given these coefficients, can we/how do we reconstruct the function?
- What accuracy can we achieve given a finite (usually small) number of coefficients?
- Computational issue – no FFT available

Problem Formulation

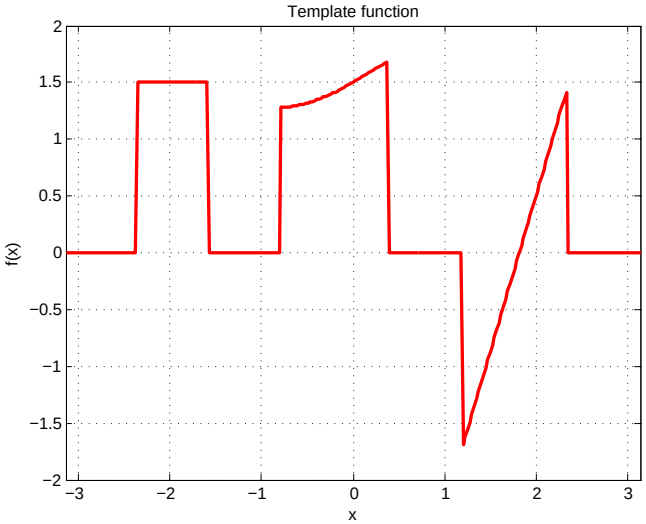

(e) Template Function

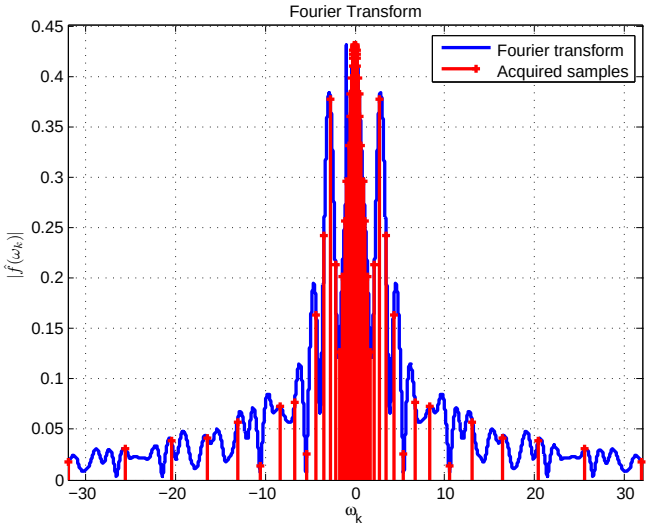

(f) Fourier Coefficients, $N = 32$

- Given these coefficients, can we/how do we reconstruct the function?
- What accuracy can we achieve given a finite (usually small) number of coefficients?
- Computational issue – no FFT available

Problem Formulation

Let f be defined on $\mathbb{R}$ and supported in $(-\pi, \pi)$ with Fourier transform

$$\hat{f}(\omega) = \frac{1}{2\pi} \int_{-\pi}^{\pi} f(x) e^{-i\omega x} dx, \quad \omega \in \mathbb{R}$$

Objective

Recover f given a finite number of its non-harmonic Fourier coefficients,

$$\hat{f}(\omega_k), \quad k = -N, ..., N \quad \omega_k \text{ not necessarily} \in \mathbb{Z}$$

- We are particularly interested in sampling patterns with variable sampling density
- The underlying function f is piecewise-smooth

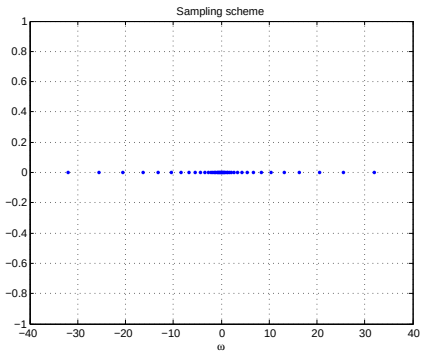

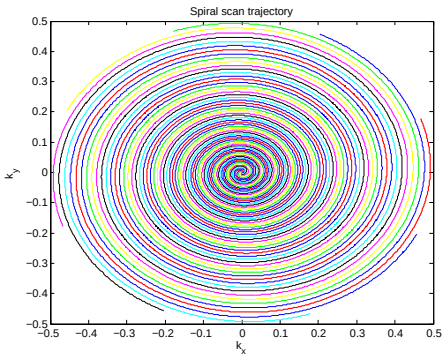

Problem Formulation

Let f be defined on $\mathbb{R}$ and supported in $(-\pi, \pi)$ with Fourier transform

$$\hat{f}(\omega) = \frac{1}{2\pi} \int_{-\pi}^{\pi} f(x) e^{-i\omega x} dx, \quad \omega \in \mathbb{R}$$

Objective

Recover f given a finite number of its non-harmonic Fourier coefficients,

$$\hat{f}(\omega_k), \quad k = -N, ..., N \quad \omega_k \text{ not necessarily} \in \mathbb{Z}$$

- We are particularly interested in sampling patterns with variable sampling density
- The underlying function f is piecewise-smooth

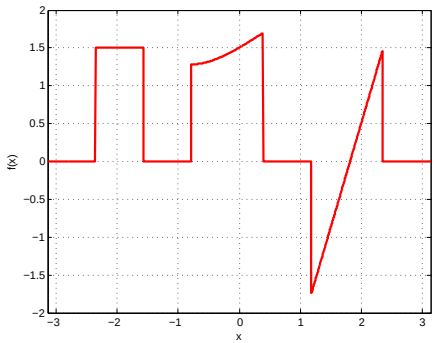

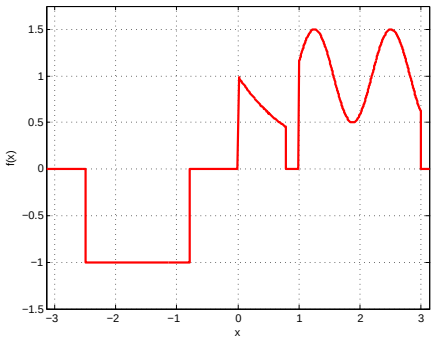

Sampling Patterns

- Jittered Sampling: $\omega_k = k \pm \tau_k, \quad \tau_k \sim U[0, \theta],\ k = -N, -(N-1), ..., N$
- Log Sampling: $|\omega_k|$ is logarithmically distributed between 10^{-v} and N, with $v > 0$ and $2N + 1$ being the total number of samples.

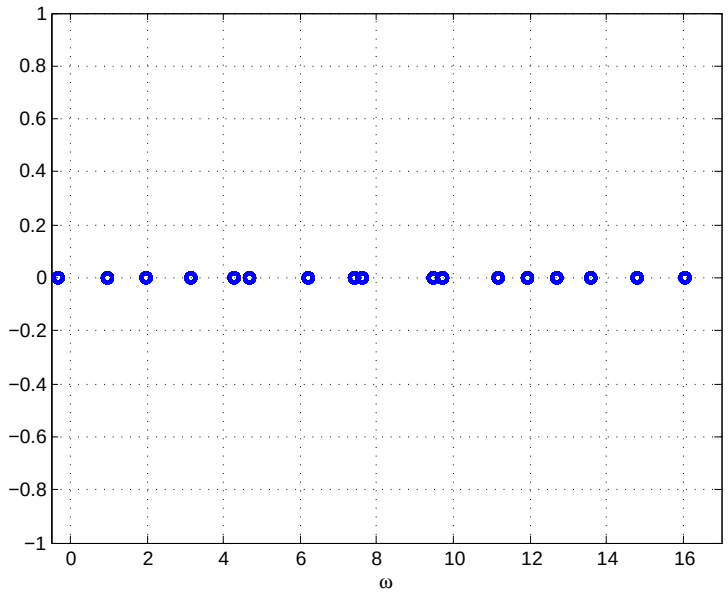

(k) Jittered Sampling

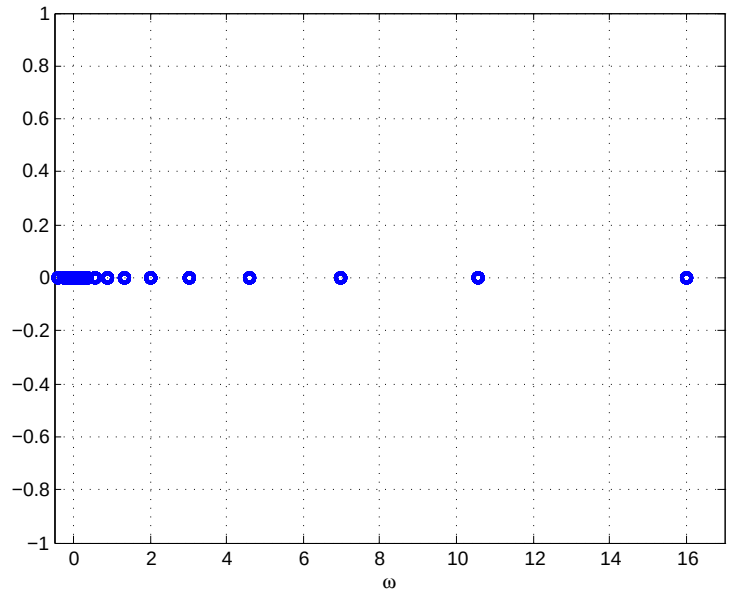

(l) Log Sampling

Figure: Non-uniform Sampling Schemes (right half plane), $N = 16$

The Non-harmonic Reconstruction Kernel

- Standard (harmonic) Fourier reconstruction:
  $S_N f(x) = \sum_{|k|\leq N} \hat{f}(k) e^{ikx} = (f * D_N)(x)$ where
  $D_N(x) = \sum_{|k|\leq N} e^{ikx}$ is the Dirichlet kernel.
- The non-harmonic Fourier reconstruction:
  $S_N \tilde{f}(x) = \sum_{|k|\leq N} \hat{f}(\omega_k) e^{i\omega_k x} = (f * A_N)(x)$ where
  $A_N(x) = \sum_{|k|\leq N} e^{i\omega_k x}$ is the non-harmonic kernel.
- The non-harmonic kernels do not constitute an orthogonal basis for span $\{e^{ikx}, |k| \leq N\}$

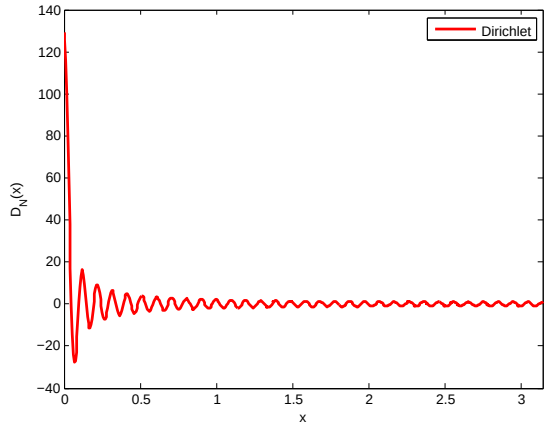

Figure: The Dirichlet Kernel plotted on the right half plane, $N = 64$

The Non-harmonic Reconstruction Kernel

- Standard (harmonic) Fourier reconstruction:
  $S_N f(x) = \sum_{|k|\leq N} \hat{f}(k) e^{ikx} = (f * D_N)(x)$ where
  $D_N(x) = \sum_{|k|\leq N} e^{ikx}$ is the Dirichlet kernel.
- The non-harmonic Fourier reconstruction:
  $S_N \tilde{f}(x) = \sum_{|k|\leq N} \hat{f}(\omega_k) e^{i\omega_k x} = (f * A_N)(x)$ where
  $A_N(x) = \sum_{|k|\leq N} e^{i\omega_k x}$ is the non-harmonic kernel.
- The non-harmonic kernels do not constitute an orthogonal basis for span $\{e^{ikx}, |k| \leq N\}$

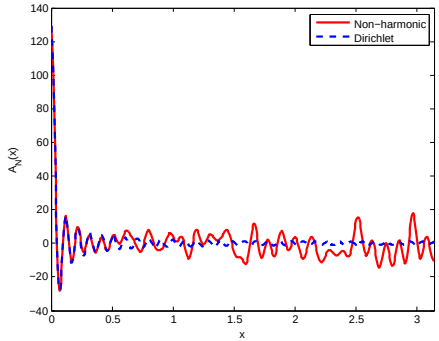

(a) Jittered Sampling

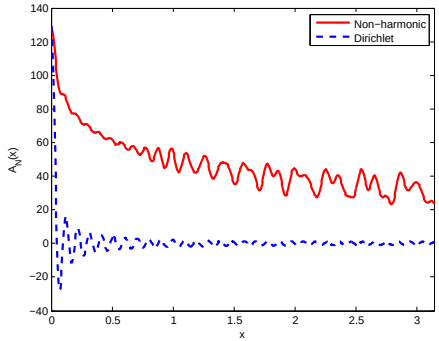

(b) Log Sampling

Figure: Non-harmonic Kernel, $N = 64$

The Non-harmonic Reconstruction Kernel

- Standard (harmonic) Fourier reconstruction:
  $S_N f(x) = \sum_{|k|\leq N} \hat{f}(k) e^{ikx} = (f * D_N)(x)$ where
  $D_N(x) = \sum_{|k|\leq N} e^{ikx}$ is the Dirichlet kernel.
- The non-harmonic Fourier reconstruction:
  $S_N \tilde{f}(x) = \sum_{|k|\leq N} \hat{f}(\omega_k) e^{i\omega_k x} = (f * A_N)(x)$ where
  $A_N(x) = \sum_{|k|\leq N} e^{i\omega_k x}$ is the non-harmonic kernel.
- The non-harmonic kernels do not constitute an orthogonal basis for span $\{e^{ikx}, |k| \leq N\}$

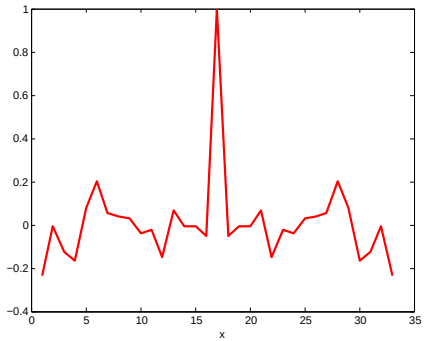

(a) Jittered Sampling

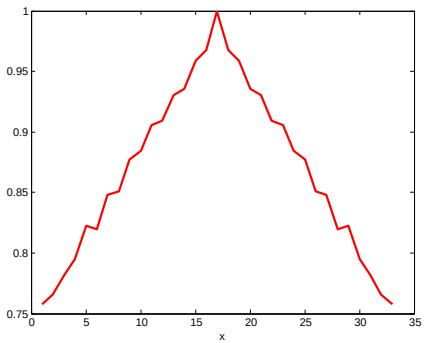

(b) Log Sampling

Figure: Autocorrelation plot of the kernels

Non-harmonic Kernels

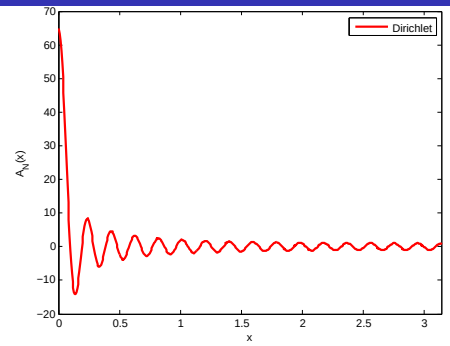

(a) Dirichlet, $N = 32$

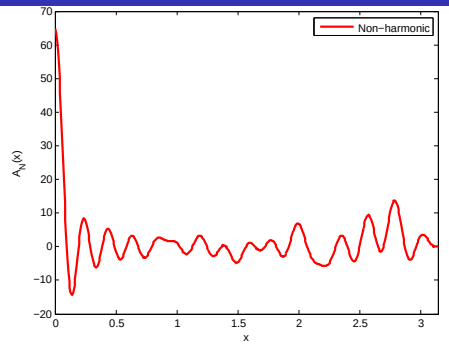

(b) Jittered, $N = 32$

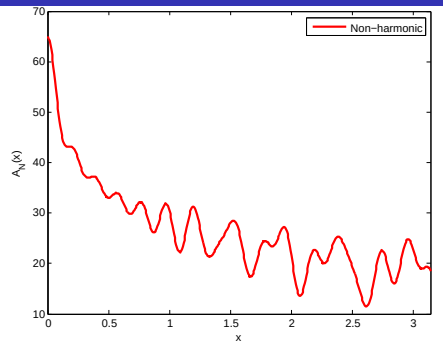

(c) Log, $N = 32$

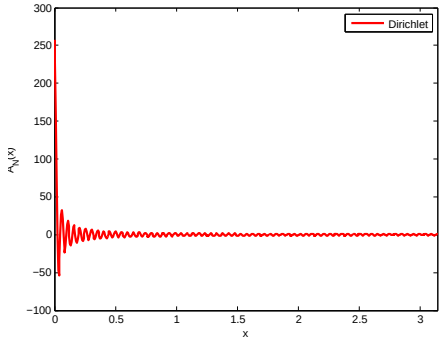

(d) Dirichlet, $N = 128$

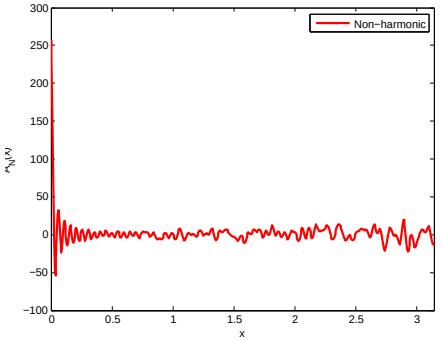

(e) Jittered, $N = 128$

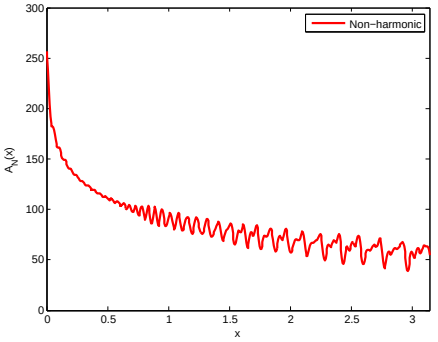

(f) Log, $N = 128$

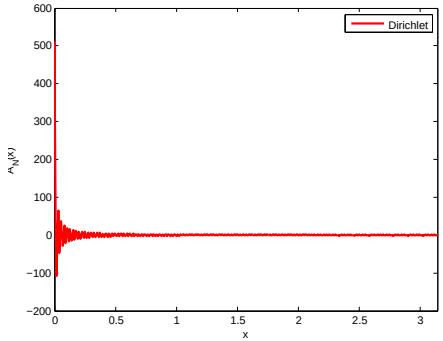

(g) Dirichlet, $N = 256$

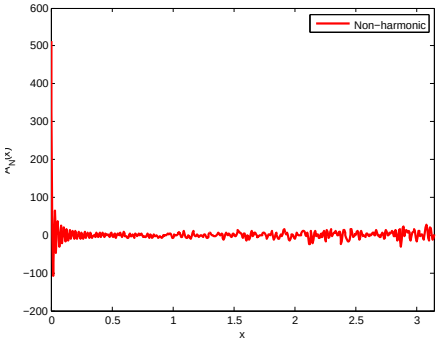

(h) Jittered, $N = 256$

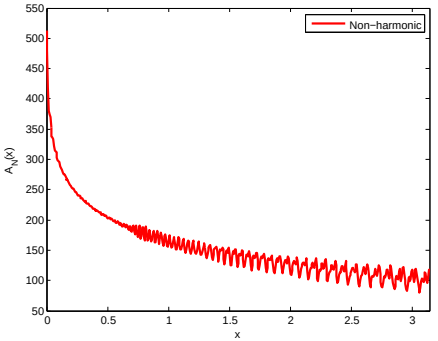

(i) Log, $N = 256$

Reconstruction Examples

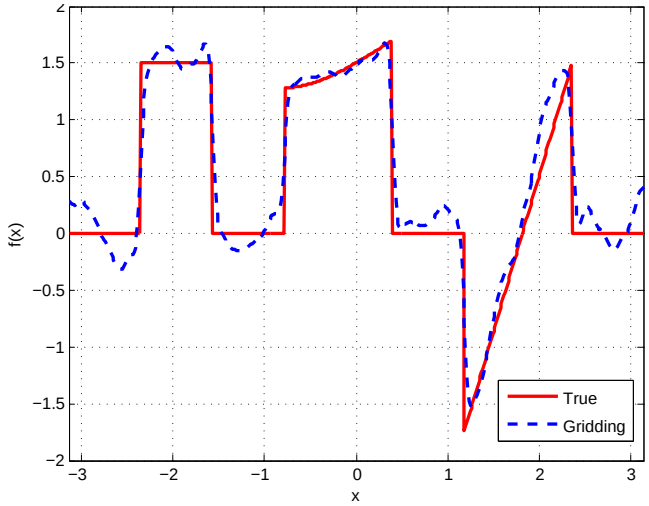

(a) "Jittered" Sampling

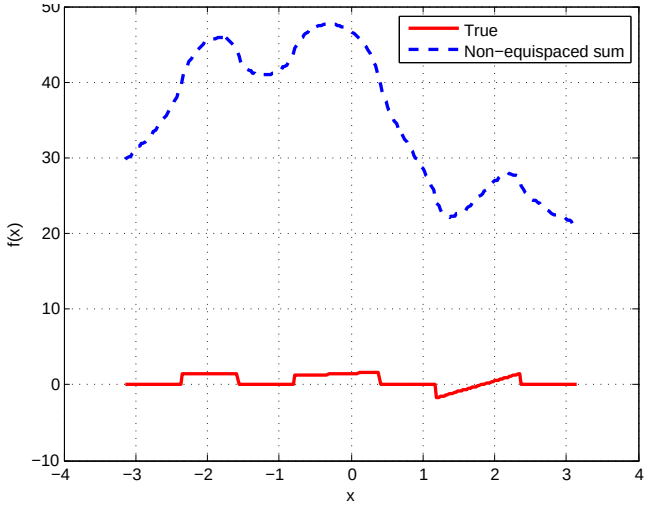

(b) "Log" Sampling

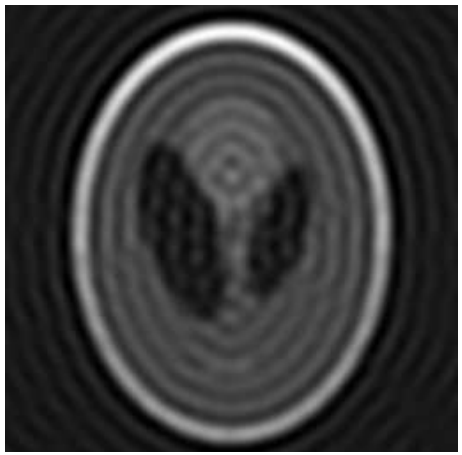

(c) "Spiral" Sampling

Figure: Non-harmonic Fourier sum Reconstruction, $N = 128$

Outline

Conventional Reconstruction Methods

Several approaches available to perform reconstruction

- Convolutional Gridding – most popular
- Uniform Resampling
- Iterative Methods

– "Fix" the quadrature rule while evaluating the non-harmonic sum

$$S_N \tilde{f}(x) = \sum_{k=-N}^{N} \alpha_k \hat{f}(\omega_k) e^{i\omega_k x}$$

– α_k are density compensation factors

e.g., $\alpha_k = \omega_{k+1} - \omega_k$

– Evaluated using a "non-uniform" FFT

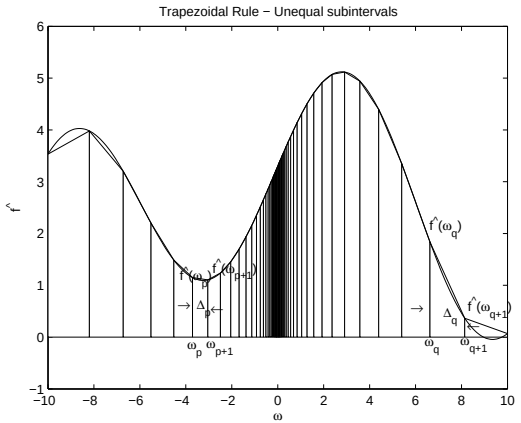

Figure: Evaluating the non-uniform Fourier sum

Although there are distinct difference in methodology and computational cost, reconstruction accuracy is similar in most schemes. We will look at convolutional gridding and uniform resampling to obtain an intuitive understanding of the problems in reconstruction.

Conventional Reconstruction Methods

Several approaches available to perform reconstruction

- Convolutional Gridding – most popular
- Uniform Resampling
- Iterative Methods

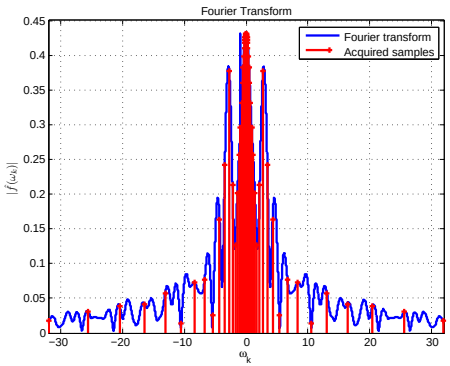

(a) Non-harmonic modes

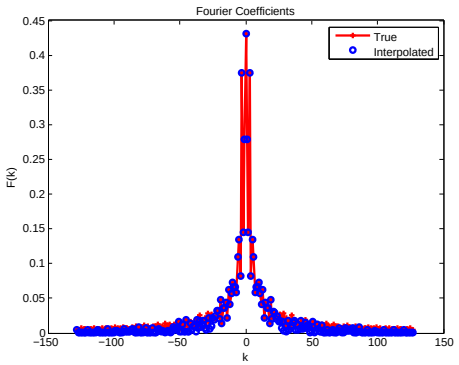

(b) Obtain uniform modes

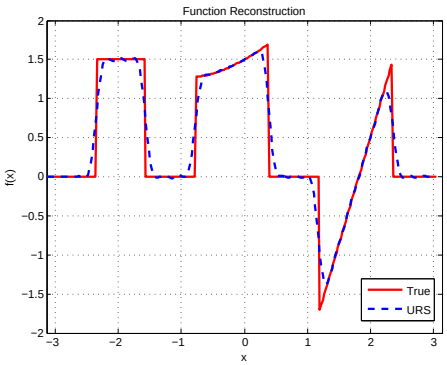

(c) (Filtered) Fourier sum

Figure: Uniform Resampling

Although there are distinct difference in methodology and computational cost, reconstruction accuracy is similar in most schemes. We will look at convolutional gridding and uniform resampling to obtain an intuitive understanding of the problems in reconstruction.

Conventional Reconstruction Methods

Several approaches available to perform reconstruction

- Convolutional Gridding – most popular
- Uniform Resampling
- Iterative Methods

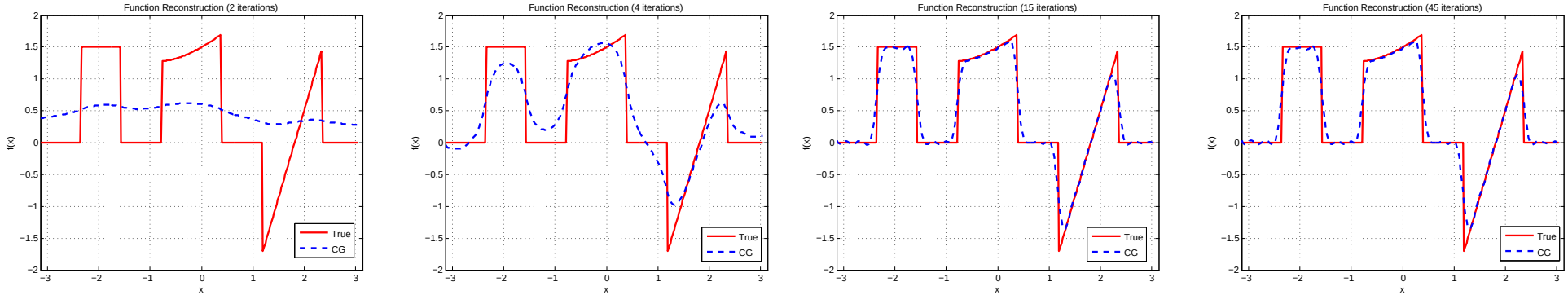

(a) after iteration 2 (b) after iteration 4 (c) after iteration 15 (d) after iteration 45

Figure: Iterative Reconstruction

Although there are distinct difference in methodology and computational cost, reconstruction accuracy is similar in most schemes. We will look at convolutional gridding and uniform resampling to obtain an intuitive understanding of the problems in reconstruction.

Conventional Reconstruction Methods

Several approaches available to perform reconstruction

- Convolutional Gridding – most popular
- Uniform Resampling
- Iterative Methods

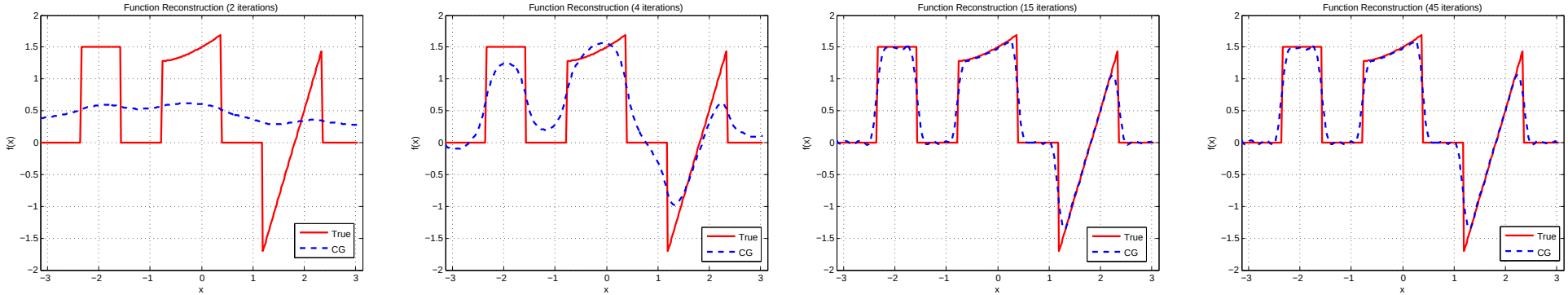

(a) after iteration 2 (b) after iteration 4 (c) after iteration 15 (d) after iteration 45

Figure: Iterative Reconstruction

Although there are distinct difference in methodology and computational cost, reconstruction accuracy is similar in most schemes. We will look at convolutional gridding and uniform resampling to obtain an intuitive understanding of the problems in reconstruction.

Convolutional Gridding

Instead of approximating f by $\sum_{k=-N}^{N} \alpha_k \hat{f}(\omega_k) e^{i\omega_k x}$, we compute

$$S_N \tilde{g}(x) = \sum_{k=-N}^{N} \hat{\tilde{g}}(k) e^{ikx}$$

1. Map the non-uniform modes to a uniform grid via convolution. The new coefficients on the uniform grid are therefore given by

$$\hat{\tilde{g}}(k) = \hat{f} * \hat{\phi}\Big|_{\omega=k} \approx \sum_{m \text{ st. } |k-\omega_m| \le q} \alpha_m \hat{f}(\omega_m) \hat{\phi}(k-\omega_m)$$

2. Compute a (filtered) Fourier partial sum.
3. "Compensate" for the mapping operation (divide by $\phi(x)$).
4. Choose the interpolating function ϕ to be *essentially bandlimited*, i.e.,

$$\begin{aligned} \hat{\phi}(\omega) &\approx 0 \quad |\omega| > q,\ q \in \mathbb{R}, \text{small} \\ \phi(x) &\approx 0 \quad |x| > \pi \\ \phi(x) &\neq 0 \quad x \in [-\pi, \pi] \end{aligned}$$

Convolutional Gridding

Instead of approximating f by $\sum_{k=-N}^{N} \alpha_k \hat{f}(\omega_k) e^{i\omega_k x}$, we compute

$$S_N \tilde{g}(x) = \sum_{k=-N}^{N} \hat{\tilde{g}}(k) e^{ikx}$$

1. Map the non-uniform modes to a uniform grid via convolution. The new coefficients on the uniform grid are therefore given by

$$\hat{\tilde{g}}(k) = \hat{f} * \hat{\phi}\Big|_{\omega=k} \approx \sum_{m \text{ st. } |k-\omega_m| \le q} \alpha_m \hat{f}(\omega_m) \hat{\phi}(k-\omega_m)$$

2. Compute a (filtered) Fourier partial sum.
3. "Compensate" for the mapping operation (divide by $\phi(x)$).
4. Choose the interpolating function ϕ to be *essentially bandlimited*, i.e.,

$$\begin{aligned} \hat{\phi}(\omega) &\approx 0 \quad |\omega| > q,\ q \in \mathbb{R}, \text{small} \\ \phi(x) &\approx 0 \quad |x| > \pi \\ \phi(x) &\neq 0 \quad x \in [-\pi, \pi] \end{aligned}$$

Convolutional Gridding

Instead of approximating f by $\sum_{k=-N}^{N} \alpha_k \hat{f}(\omega_k) e^{i\omega_k x}$, we compute

$$S_N \tilde{g}(x) = \sum_{k=-N}^{N} \hat{\tilde{g}}(k) e^{ikx}$$

1. Map the non-uniform modes to a uniform grid via convolution. The new coefficients on the uniform grid are therefore given by

$$\hat{\tilde{g}}(k) = \hat{f} * \hat{\phi}\Big|_{\omega=k} \approx \sum_{m \text{ st. } |k-\omega_m| \le q} \alpha_m \hat{f}(\omega_m) \hat{\phi}(k-\omega_m)$$

2. Compute a (filtered) Fourier partial sum.
3. "Compensate" for the mapping operation (divide by $\phi(x)$).
4. Choose the interpolating function ϕ to be *essentially bandlimited*, i.e.,

$$\begin{aligned} \hat{\phi}(\omega) &\approx 0 \quad |\omega| > q,\ q \in \mathbb{R}, \text{small} \\ \phi(x) &\approx 0 \quad |x| > \pi \\ \phi(x) &\neq 0 \quad x \in [-\pi, \pi] \end{aligned}$$

Convolutional Gridding

Instead of approximating f by $\sum_{k=-N}^{N} \alpha_k \hat{f}(\omega_k) e^{i\omega_k x}$, we compute

$$S_N \tilde{g}(x) = \sum_{k=-N}^{N} \hat{\tilde{g}}(k) e^{ikx}$$

1. Map the non-uniform modes to a uniform grid via convolution. The new coefficients on the uniform grid are therefore given by

$$\hat{\tilde{g}}(k) = \hat{f} * \hat{\phi}\Big|_{\omega=k} \approx \sum_{m \text{ st. } |k-\omega_m| \le q} \alpha_m \hat{f}(\omega_m) \hat{\phi}(k-\omega_m)$$

2. Compute a (filtered) Fourier partial sum.
3. "Compensate" for the mapping operation (divide by $\phi(x)$).
4. Choose the interpolating function ϕ to be *essentially bandlimited*, i.e.,

$$\begin{aligned} \hat{\phi}(\omega) &\approx 0 \quad |\omega| > q,\ q \in \mathbb{R}, \text{small} \\ \phi(x) &\approx 0 \quad |x| > \pi \\ \phi(x) &\neq 0 \quad x \in [-\pi, \pi] \end{aligned}$$

Convolutional Gridding

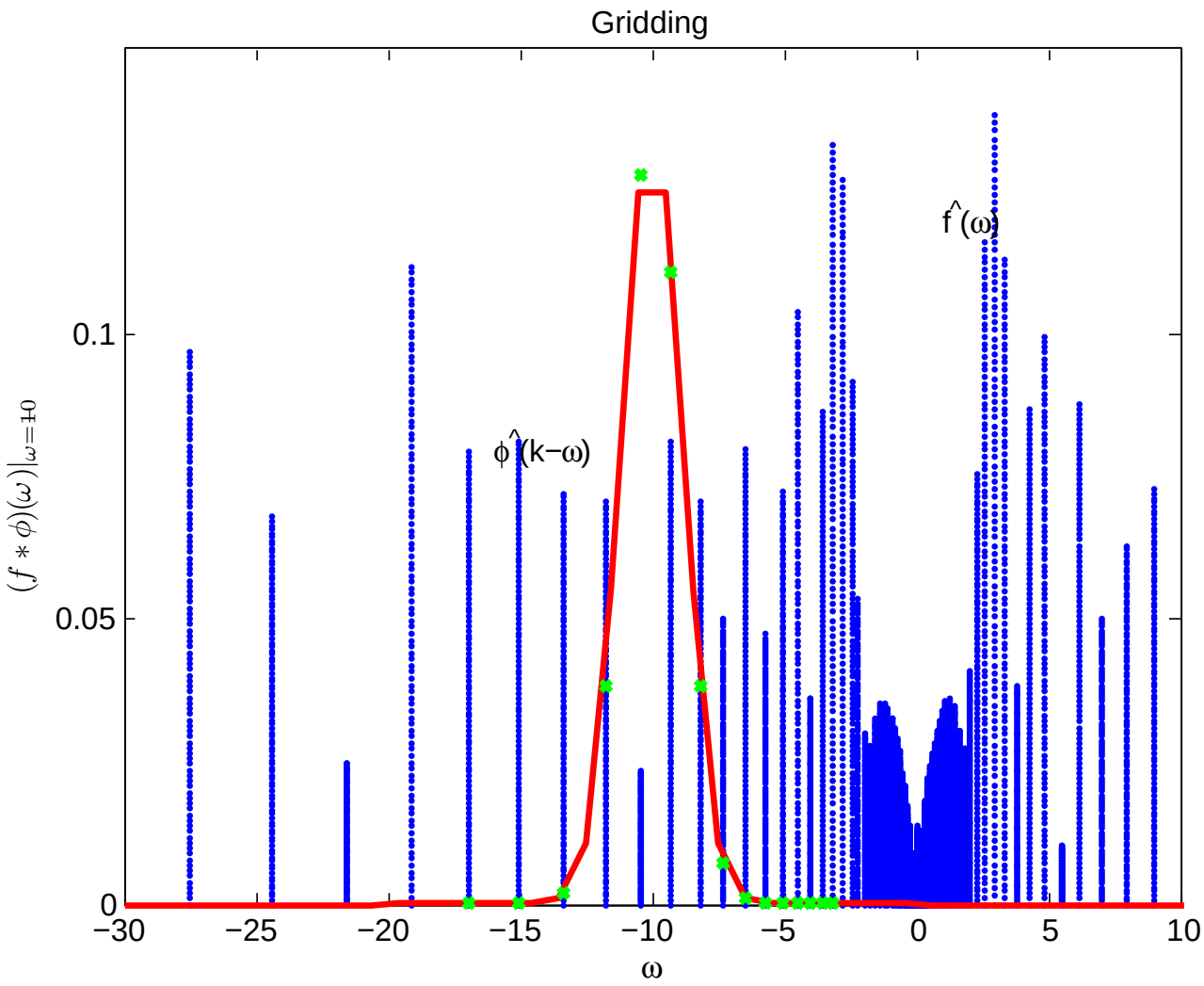

Figure: Gridding: $\hat{\tilde{g}} = \hat{f} * \hat{\phi}$

Convolutional Gridding

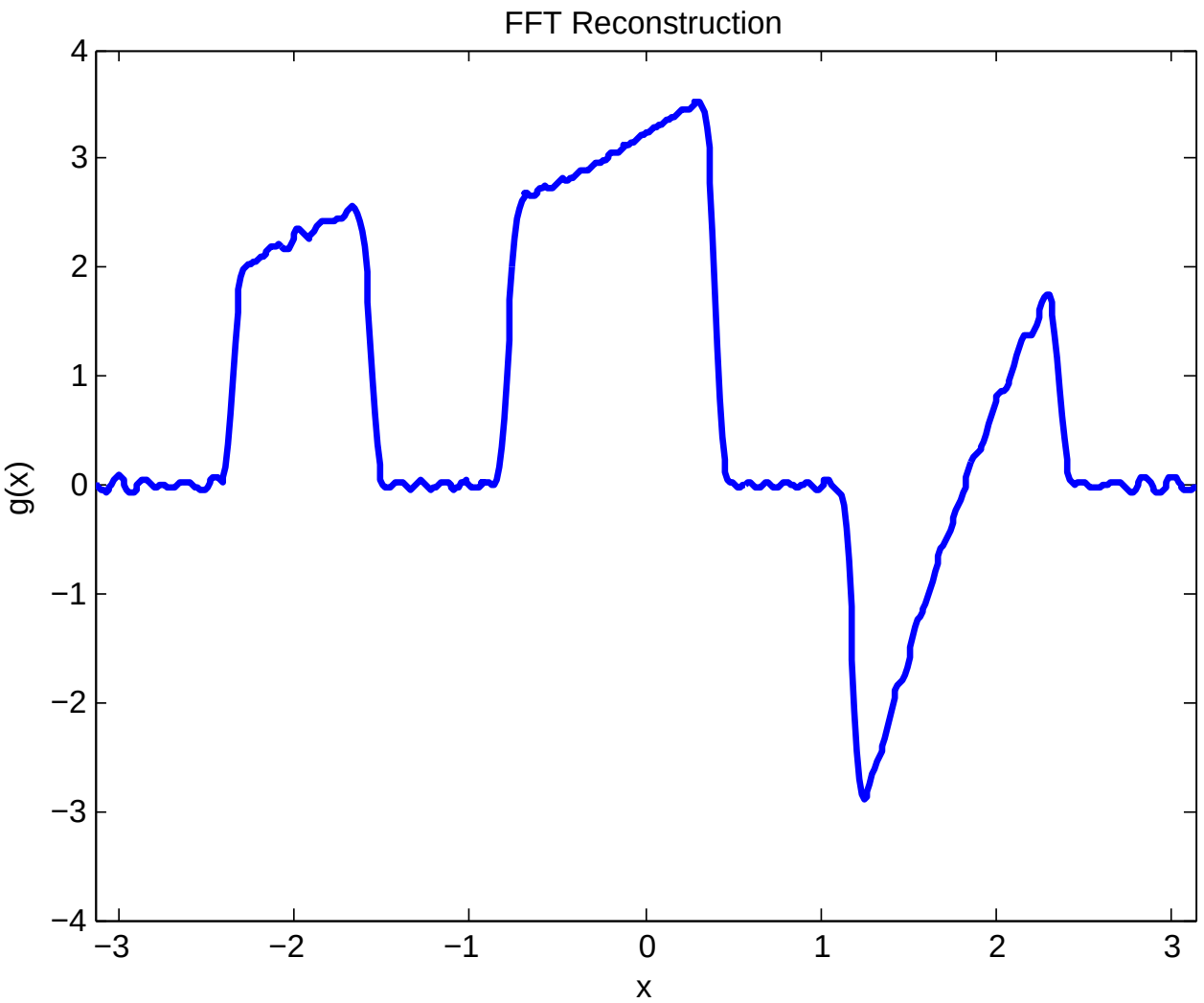

Figure: Fourier Reconstruction of $g(x) = f(x)\phi(x)$

Convolutional Gridding

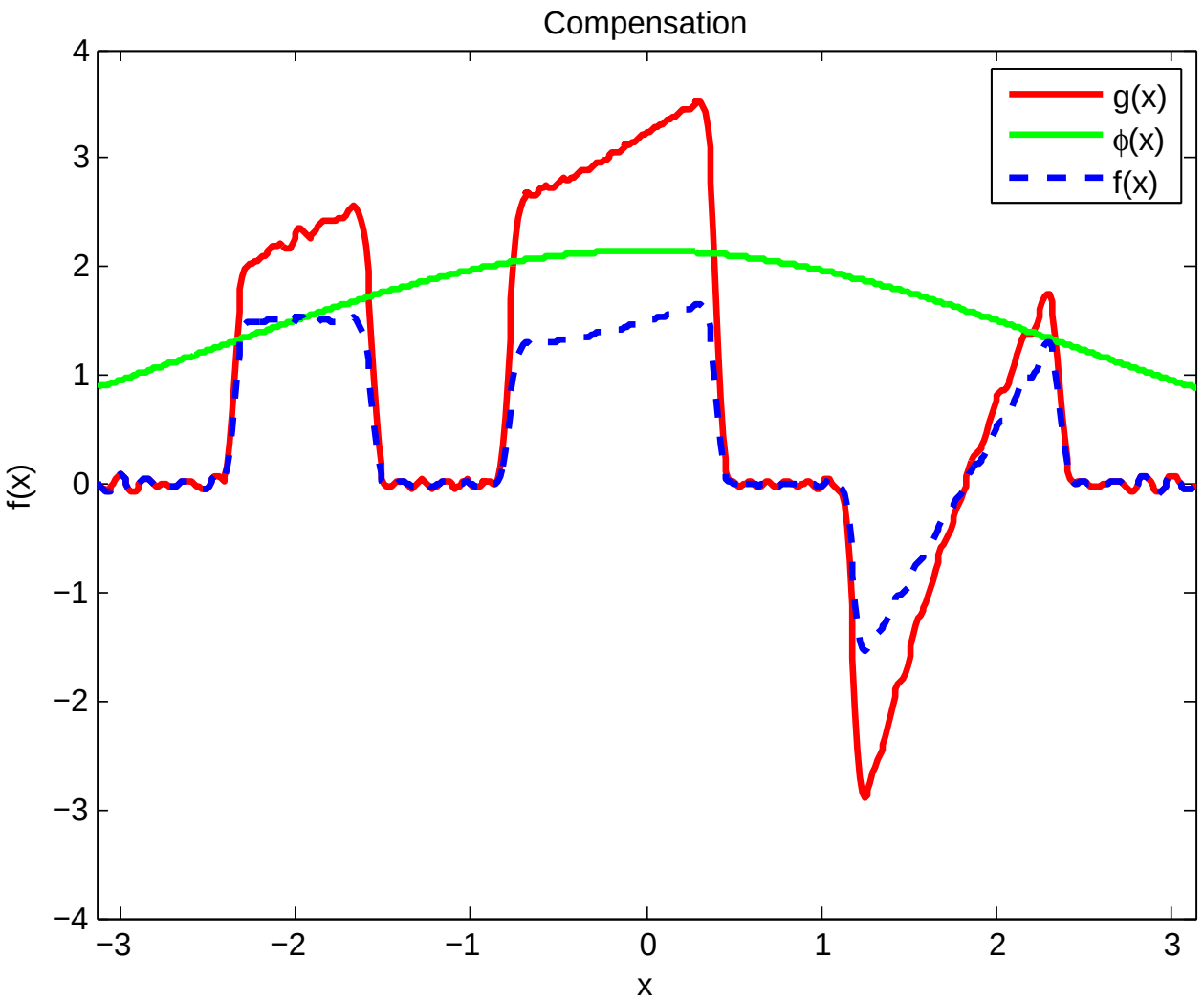

Figure: Compensation $f(x) = g(x)/\phi(x)$

Reconstruction Examples – Convolutional Gridding

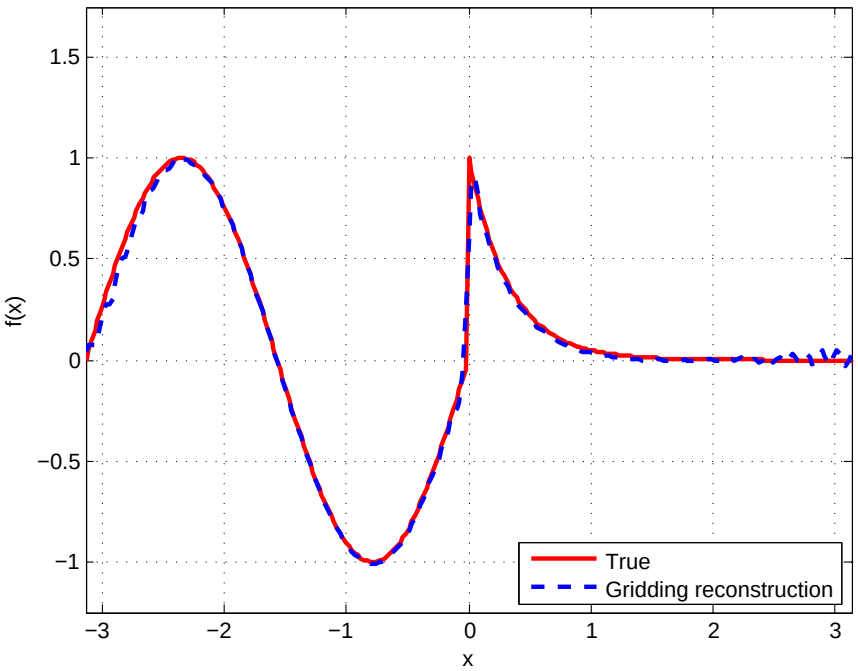

(a) Test Function reconstruction

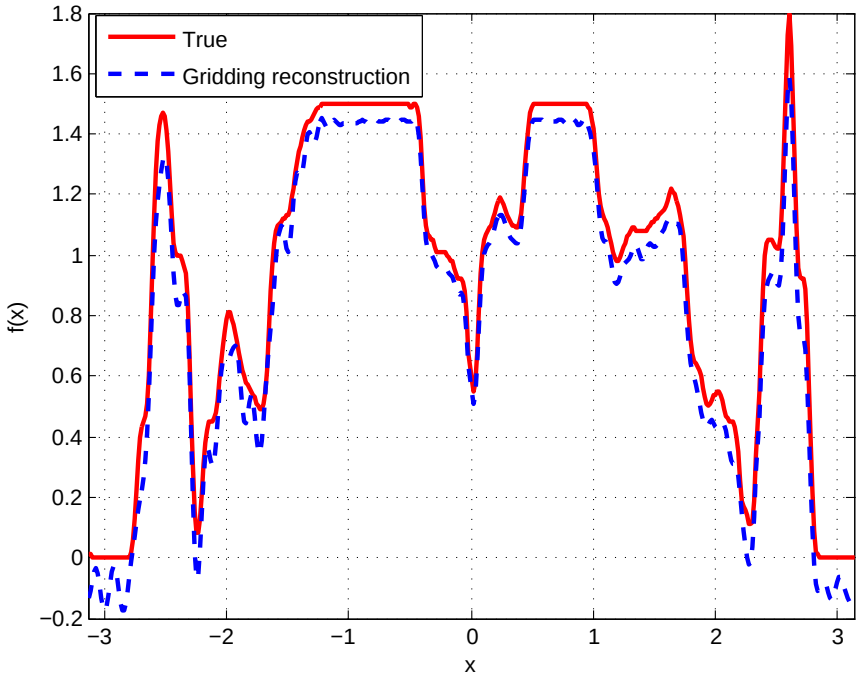

(b) Cross-section of a brain scan

Figure: Gridding reconstruction, $N = 128$ (processed by a fourth order exponential filter)

Uniform Resampling

Reconstruction is accomplished in two steps:

1. recover equispaced coefficients $\hat{f}(k)$
2. partial Fourier reconstruction using the FFT algorithm

Since f is compactly supported, we use the sampling theorem to relate $\hat{f}(\omega_k)$ and $\hat{f}(k)$.

$$\hat{f}(\omega) = \sum_{p=-\infty}^{\infty} \hat{f}(p)\,\mathrm{sinc}(\omega - p), \quad \omega \in \mathbb{R}, p \in \mathbb{N}$$

- To recover $\hat{f}(k)$, we have to invert the above system, i.e., solve

$$Ax = b, \quad A_{ij} = \mathrm{sinc}(\omega_i - j), \quad b = \left\{\hat{f}(\omega_k)\right\}_{k=-N}^{N}, \quad x = \left\{\hat{f}(p)\right\}_{p=-M}^{M}$$

- Any number of methods to do so - iterative methods, pseudoinverse-based methods with regularization ...
- The condition number of the sinc matrix depends on the sampling pattern's deviation from equispaced nodes.

Representative Results – Uniform Resampling

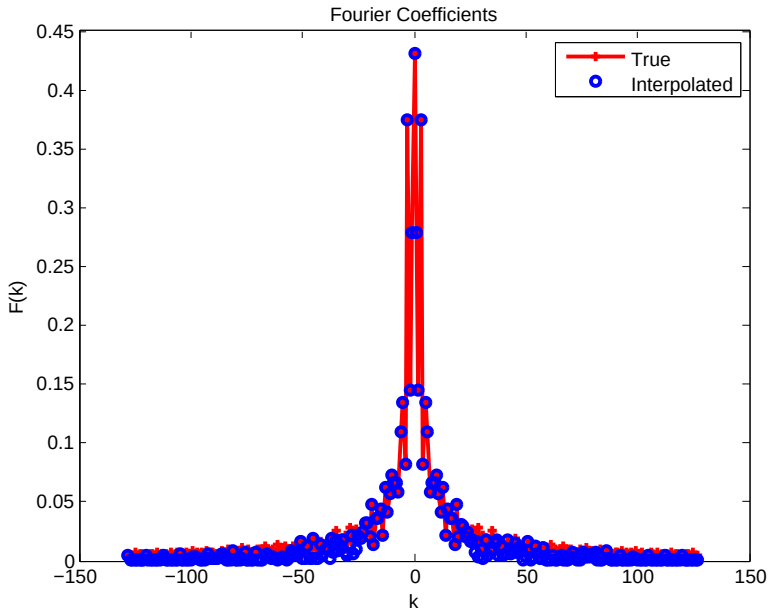

(a) Recovered Fourier coefficients

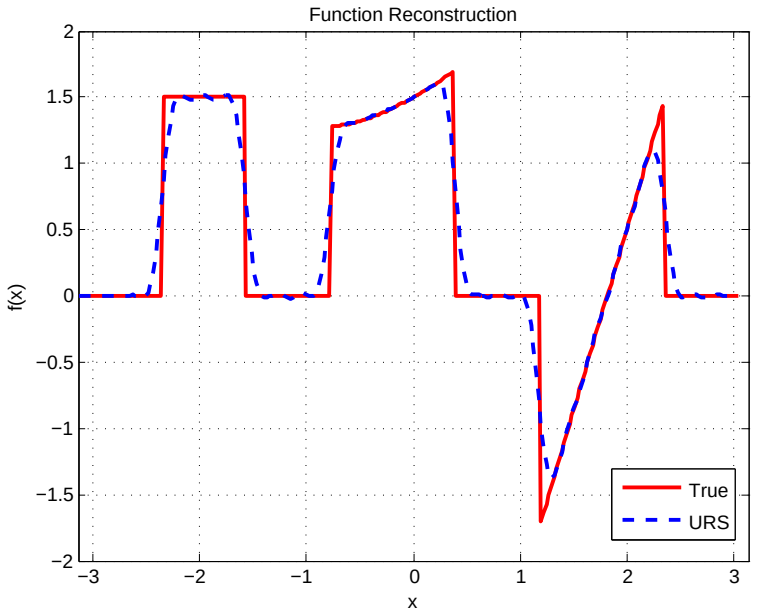

(b) Filtered reconstruction

Figure: URS solution, $N = 128$

- Solved a square 128×128 system
- Inverted the system by computing the pseudoinverse
- Pseudoinverse was computed using TSVD, with a SVD threshold of 10^{-5}

Convolutional Gridding Error

Theorem (Convolutional Gridding Error (Viswanathan, 2009))

Let $\hat{g} = \hat{f} * \hat{\phi}$ denote the true gridding coefficients and $\hat{\tilde{g}}$ denote the approximate gridding coefficients. Let Δ_k be the maximum distance between sampling points and $d_k := \frac{1}{\Delta_k}$ be the minimum sample density in the q-vicinity of k. Then, the gridding error at mode k is bounded by $e(k) \leq C \cdot \frac{1}{d_k^2}$, $k = -N, ..., N$ for some positive constant C.

Convolutional Gridding Error

Physical space reconstruction error

$$\begin{aligned} e(x) \approx g(x) - S_N\tilde{g}(x) &= g(x) - S_N g(x) + S_N g(x) - S_N\tilde{g}(x) \\ &= \underbrace{\sum_{|k|>N} \hat{g}(k)e^{ikx}}_{\text{standard Fourier truncation}} + \underbrace{\sum_{|k|\leq N} \left(\hat{g}(k) - \hat{\tilde{g}}(k)\right) e^{ikx}}_{\text{gridding}} \end{aligned}$$

- $S_N g$ suffers from Gibbs; the maximum error occurs in the vicinity of a jump (≈ 1.09 of the jump value). There is also a reduced rate of convergence with $\|g - S_N g\| = \mathcal{O}(N)$.
- Gridding (sampling) error

$$\begin{aligned} |S_N g(x) - S_N\tilde{g}(x)| &= \left| \sum_{|k|\leq N} \left(\hat{g}(k) - \hat{\tilde{g}}(k)\right) e^{ikx} \right| \\ &\leq \sum_{|k|\leq N} \left|\hat{g}(k) - \hat{\tilde{g}}(k)\right| \\ &\leq C \sum_{|k|\leq N} \frac{1}{d_k^2} \end{aligned}$$

Error Plots

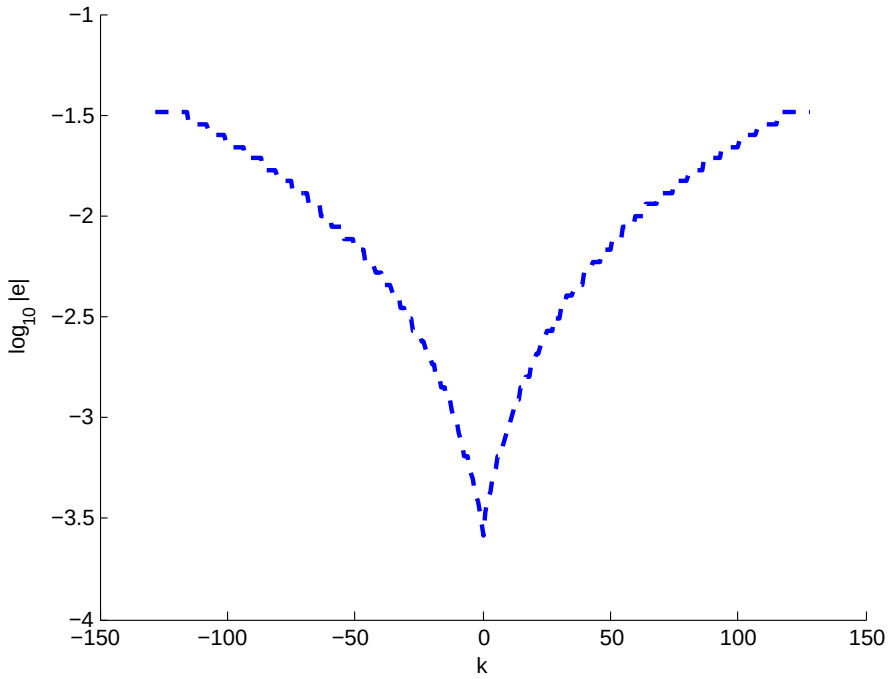

(a) Error bound, log sampling

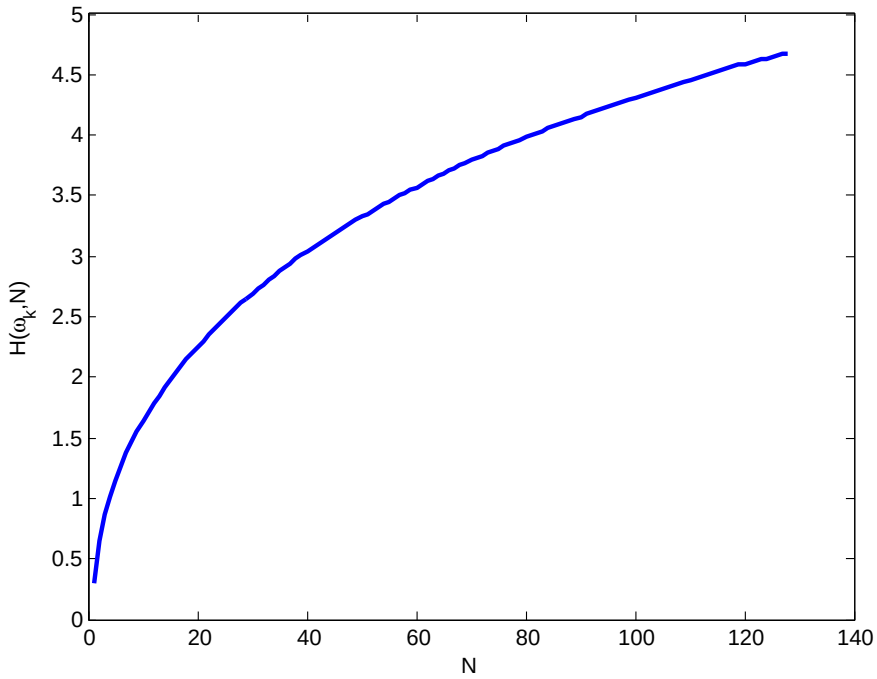

(b) $|S_N g(x) - S_N \tilde{g}(x)|$ vs N

Figure: Error Plots

Error Plots

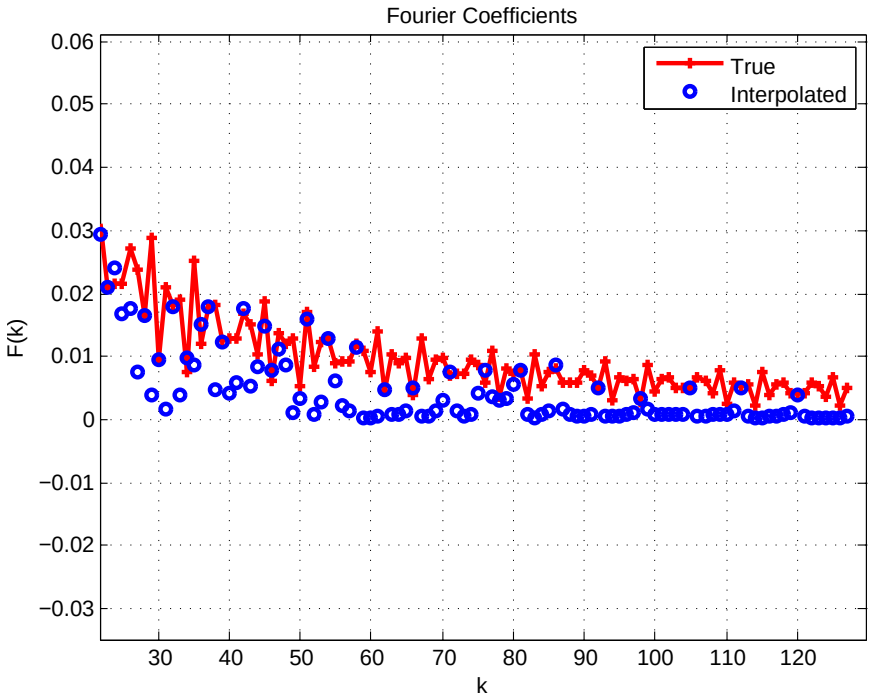

(a) Fourier coefficients – High modes

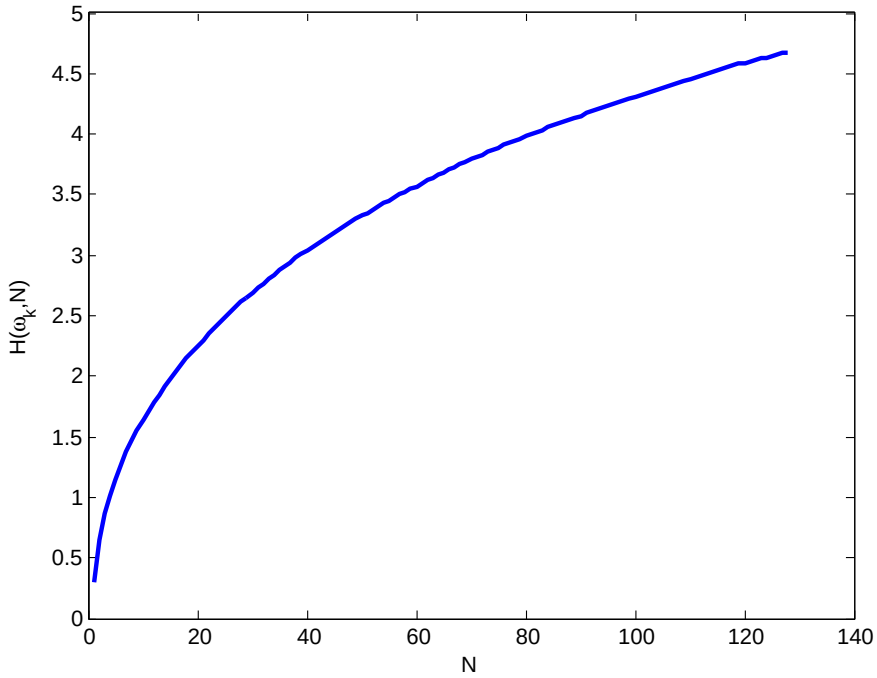

(b) $|S_N g(x) - S_N \tilde{g}(x)|$ vs N

Figure: Error Plots

Error vs Sampling Density

The reconstruction error is

$$e(x) \approx \sum_{|k|>N} \hat{g}(k) e^{ikx} + \sum_{|k|\leq N} \left(\hat{g}(k) - \hat{\tilde{g}}(k) \right) e^{ikx}$$

- 1^{st} term decreases as N increases
- 2^{nd} term increases as N increases

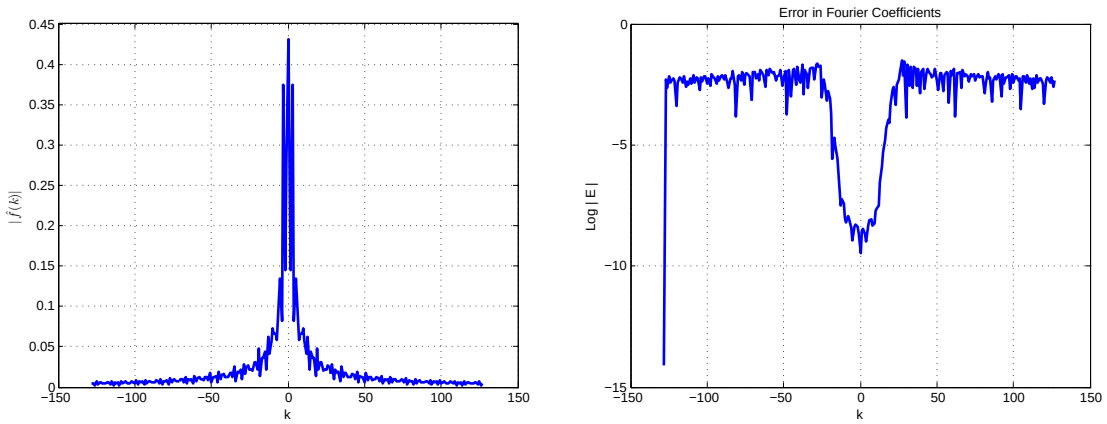

(a) Fourier coefficients (b) Coefficient error

Figure: Error in gridding coefficients

For a given sampling trajectory and function, there is a critical value N_{crit} beyond which adding coefficients does not improve the accuracy.
While filtering decreases the error, the underlying problem is not solved.

Error vs Sampling Density

The reconstruction error is

$$e(x) \approx \sum_{|k|>N} \hat{g}(k) e^{ikx} + \sum_{|k|\leq N} \left(\hat{g}(k) - \hat{\tilde{g}}(k) \right) e^{ikx}$$

- 1^{st} term decreases as N increases
- 2^{nd} term increases as N increases

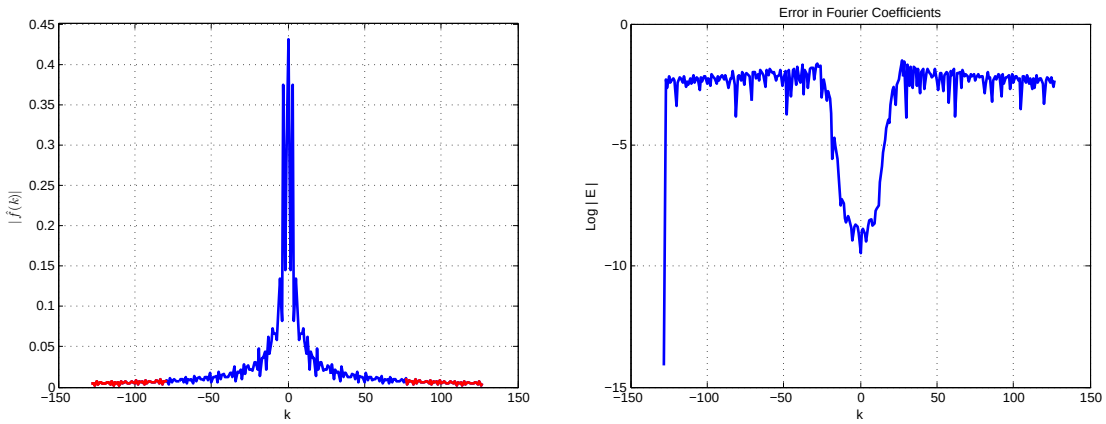

(a) Fourier coefficients (b) Coefficient error

Figure: Error in uniform re-sampling

For a given sampling trajectory and function, there is a critical value N_{crit} beyond which adding coefficients does not improve the accuracy.
While filtering decreases the error, the underlying problem is not solved.

Error vs Sampling Density

The reconstruction error is

$$e(x) \approx \sum_{|k|>N} \hat{g}(k) e^{ikx} + \sum_{|k|\leq N} \left(\hat{g}(k) - \hat{\tilde{g}}(k) \right) e^{ikx}$$

- 1^{st} term decreases as N increases
- 2^{nd} term increases as N increases

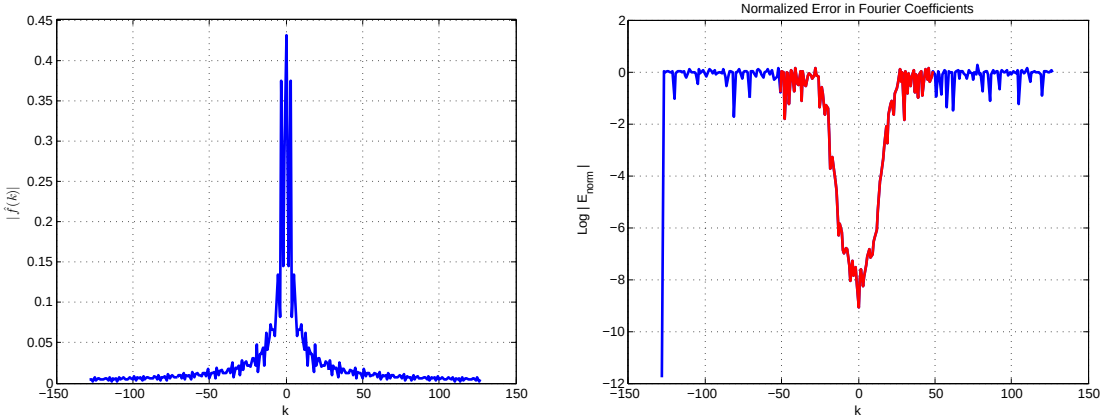

(a) Fourier coefficients (b) Coefficient error

Figure: Error in uniform re-sampling

For a given sampling trajectory and function, there is a critical value N_{crit} beyond which adding coefficients does not improve the accuracy.
While filtering decreases the error, the underlying problem is not solved.

Error in Recovered Coefficients – Uniform Resampling

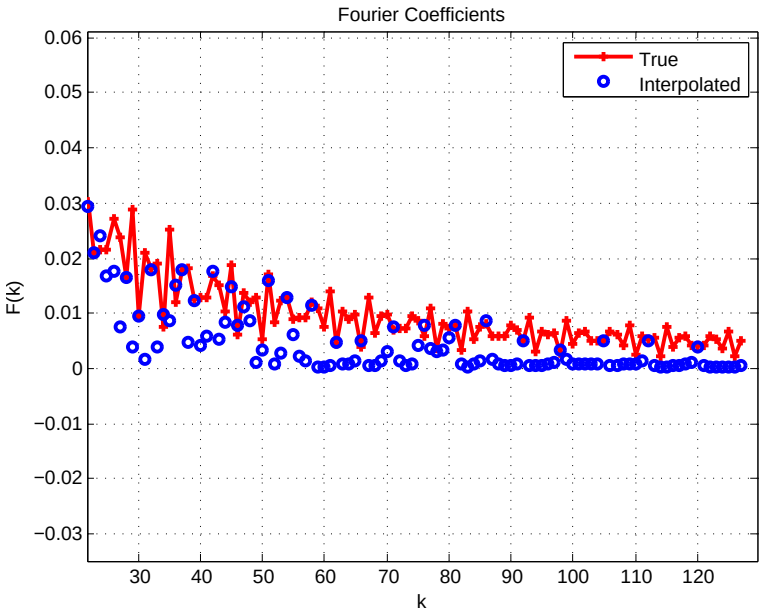

(a) Recovered Fourier coefficients

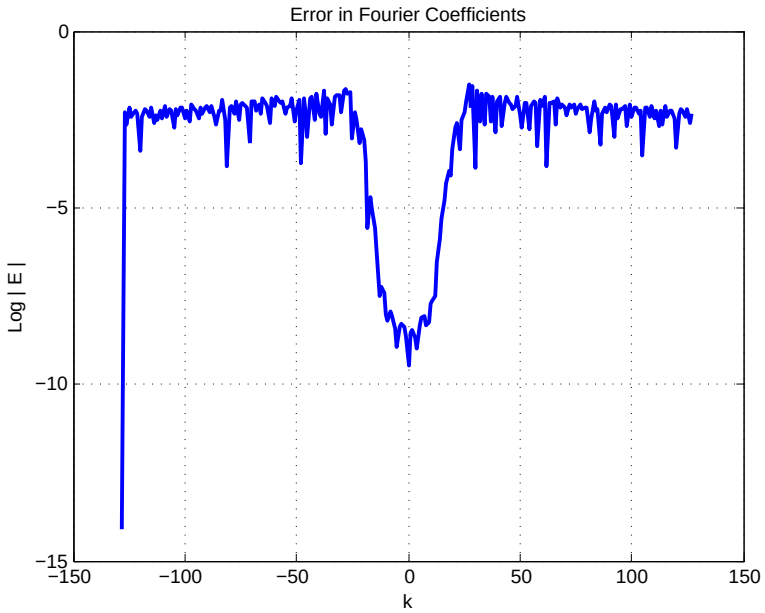

(b) Error in recovered coefficients

Figure: URS solution, $N = 128$

- The condition number of the resampling matrix is directly related to the error in the coefficients.

Outline

Gibbs Phenomenon, non-uniform case

- We still have the "Gibbs phenomenon" – non-physical oscillations at discontinuities, and a reduced rate of convergence (first order). Hence, we require a large number of coefficients to get acceptable reconstructions.
- However, by formulation of the sampling scheme and recovery procedure, the coefficients recovered at large ω are inaccurate.

$\Longrightarrow$ we need more coefficients, but the coefficients we get are inaccurate!

Spectral Reprojection – High frequency modes of f in the original basis have exponentially small contributions on the low modes in the new basis

Reducing the Impact of the High Mode Coefficients using Spectral Reprojection (Viswanathan, Cochran, Gelb, & Renaut, 2010)

Spectral reprojection expansion coefficients:

$$\frac{1}{\gamma_l^\lambda} < S_N\tilde{g}, C_l^\lambda >_{\omega(\lambda)} = \frac{1}{\gamma_l^\lambda}\int_{-1}^{1}(1-\eta^2)^{\lambda-1/2}C_l^\lambda(\eta)\sum_{|k|\le N}\hat{\tilde{g}}(k)e^{i\pi k\eta}d\eta$$

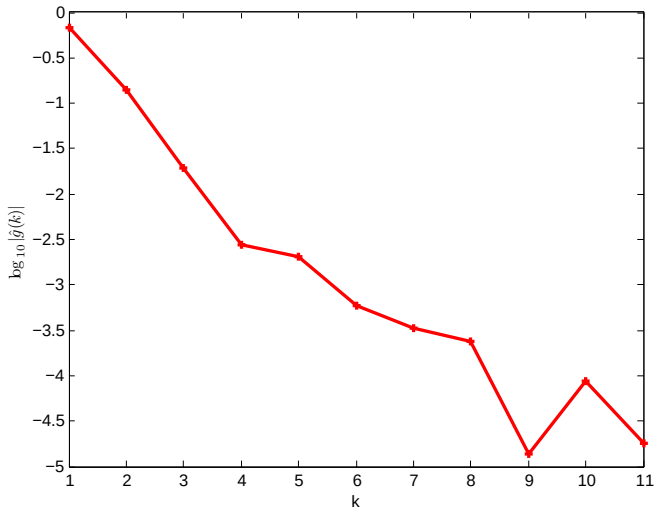

Figure: Decay of Gegenbauer coefficients

Spectral Reprojection Error of Gridded Coefficients

- $Err(m, N, g, \omega) := ||g - P_m(S_N \tilde{g})|| \leq$
  $||g - P_m g|| + ||P_m(g - S_N g)|| + ||P_m S_N g - P_m S_N \tilde{g}||$
- $||P_m S_N g - P_m S_N \tilde{g}||_\infty \leq$
  $Const \sum_{l=0}^{m} \sum_{|k| \leq N} \frac{1}{d_k^2} \left| \frac{C_l^\lambda(1)}{\gamma_l^\lambda} \int_{-1}^{1} (1-\eta^2)^{\lambda - 1/2} C_l^\lambda(\eta) e^{i\pi k \eta} d\eta \right|$
-
$$\left| \frac{C_l^\lambda(1)}{\gamma_l^\lambda} \int_{-1}^{1} (1-\eta^2)^{\lambda-1/2} C_l^\lambda(\eta) e^{i\pi k\eta} d\eta \right| \leq \frac{\Gamma(\lambda)(l+\lambda)\Gamma(l+2\lambda)}{l!\Gamma(2\lambda)} \left(\frac{2}{\pi|k|} \right)^\lambda$$
- The corresponding gridding error does not increase rapidly with N

Spectral Reprojection – Contribution from Gridding Error

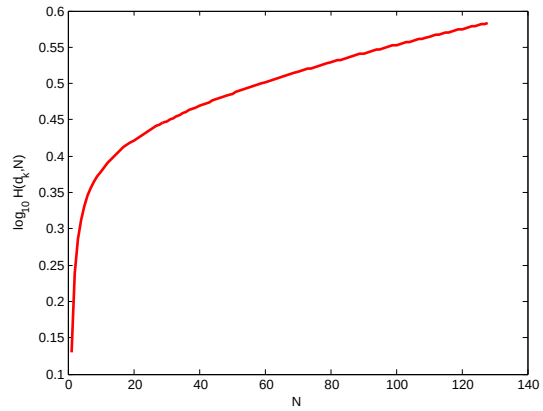

(a) Gridding Error $\lambda = 2$

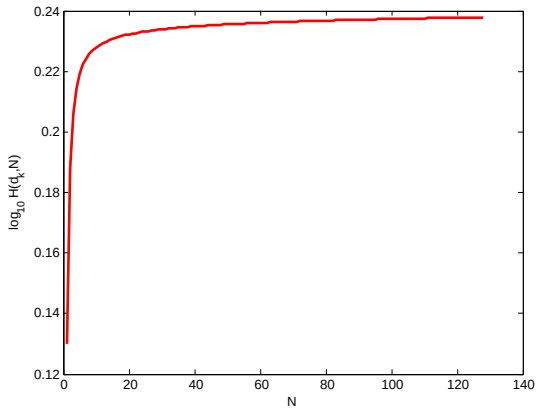

(b) Gridding Error $\lambda = 3$

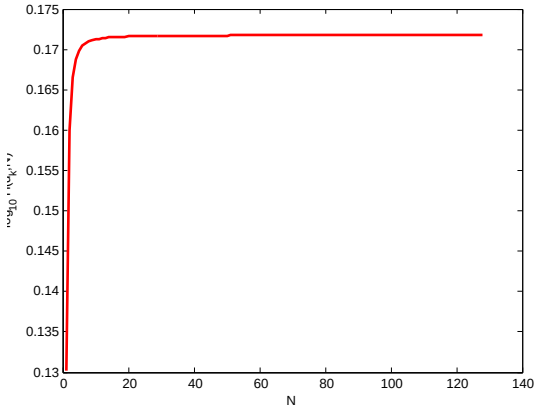

(c) Gridding Error $\lambda = 4$

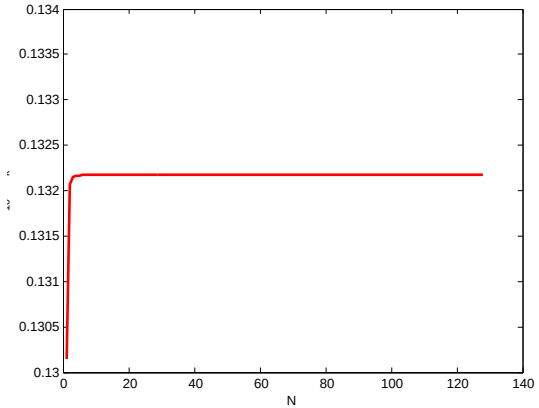

(d) Gridding Error $\lambda = 8$

Figure: Contribution from Gridding Error in Spectral Reprojection

Gegenbauer Reconstruction - Results

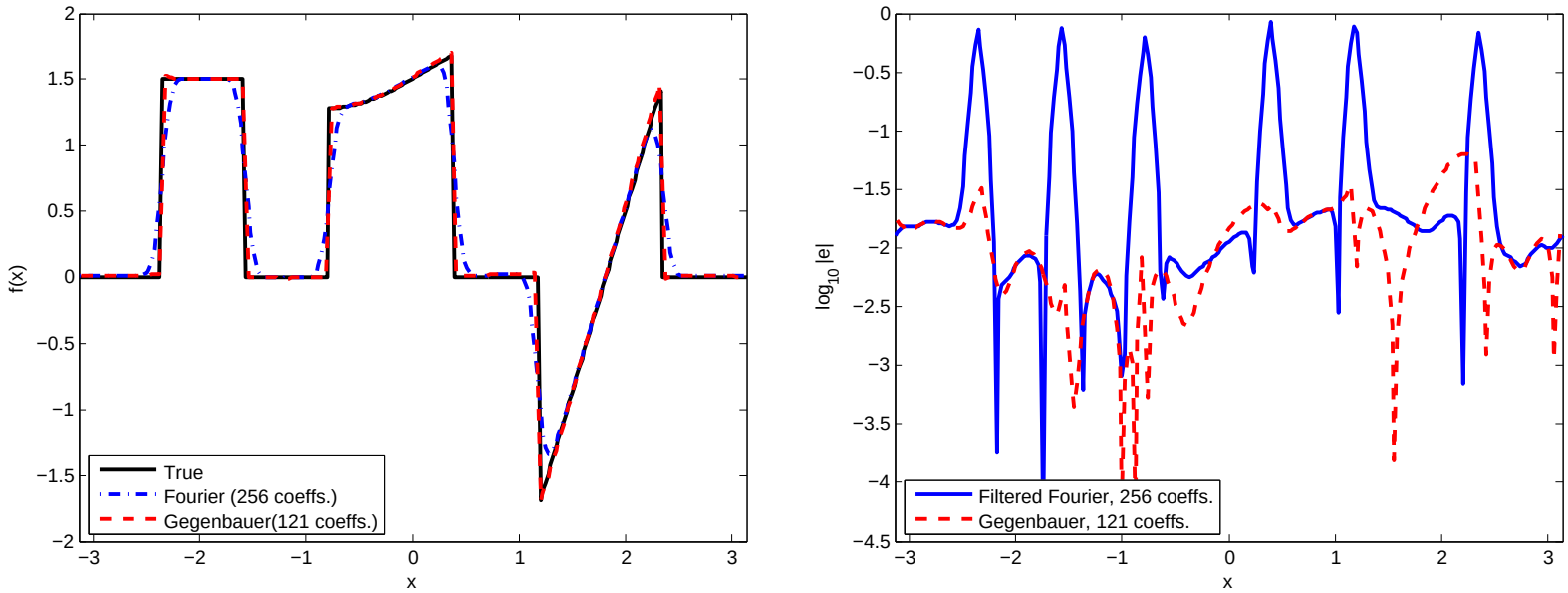

(a) Reconstruction

(b) Reconstruction error

Figure: Gegenbauer reconstruction from log spectral samples

- Filtered Fourier (second-order exponential) reconstruction uses 256 coefficients
- Gegenbauer reconstruction uses $2N + 1 = 121$ coefficients
- Edges detected using the concentration method (Gelb & Tadmor) with thresholding and non-linear post-processing.
- Parameters (m, λ) chosen proportional to size of reconstruction interval.

Error Plots

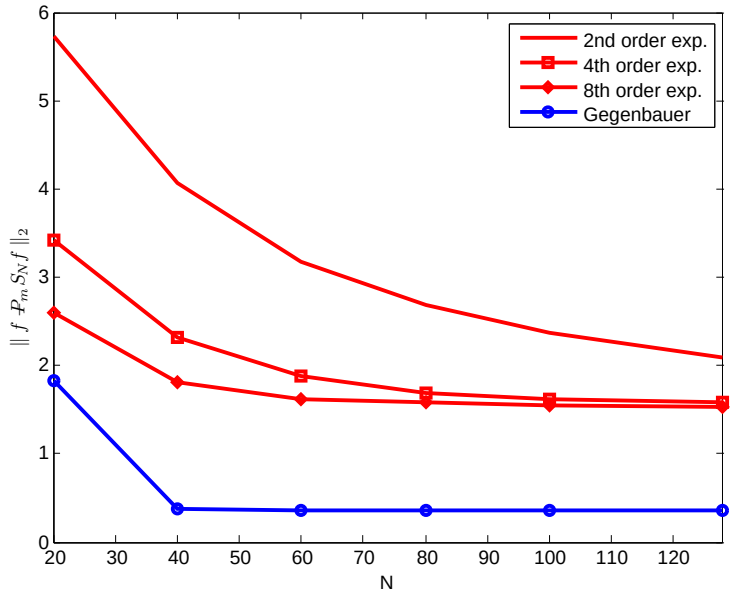

(a) 2-norm error

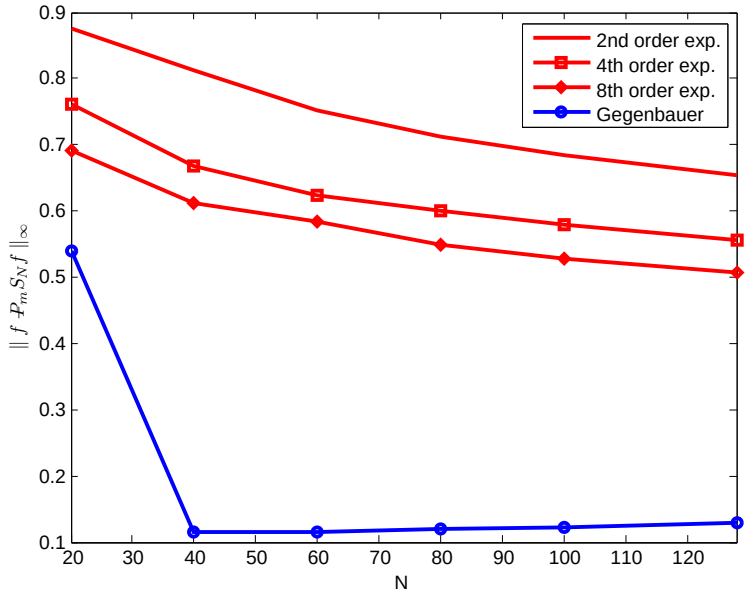

(b) Maximum-norm error

Figure: Error Plots – Filtered and Gegenbauer Reconstruction

Incorporating Edge Information into Reconstruction (Viswanathan, 2010)

Obtain edge information by

- Using the concentration method on the recovered coefficients

$$S_N^{\sigma}[\tilde{f}](x) = i \sum_{k=-N}^{N} \hat{\tilde{f}}(k)\,\mathrm{sgn}(k)\,\sigma\left(\frac{|k|}{N}\right) e^{ikx}$$

- Solving for the jump function directly from the non-harmonic Fourier data
  Let $\breve{f}(\omega_k) = i\,\mathrm{sgn}(\omega_k)\hat{f}(\omega_k)$

$$\min_{p} \quad \| \mathcal{F}\{Wp\}|_{\omega_k} - \breve{f}(\omega_k) \|_2^2 + \lambda \| p \|_1$$

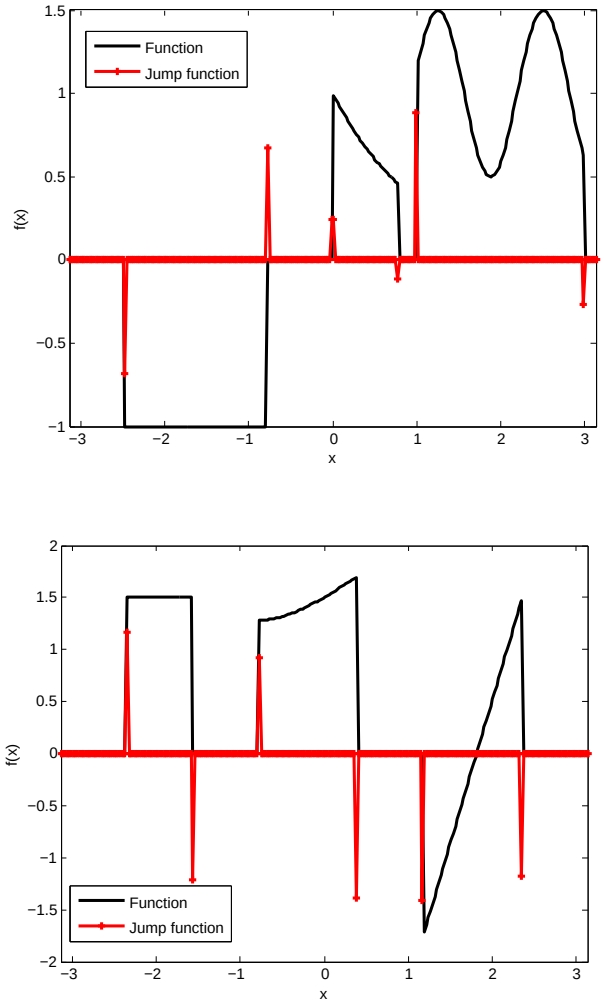

Figure: Edge Detection using the iterative formulation

Methods Incorporating Edge Information

- Compute the high frequency modes using the relation Compare

$$\hat{f}(k) = \sum_{p \in \mathcal{P}} [f](\zeta_p) \frac{e^{-ik\zeta_p}}{2\pi ik}$$

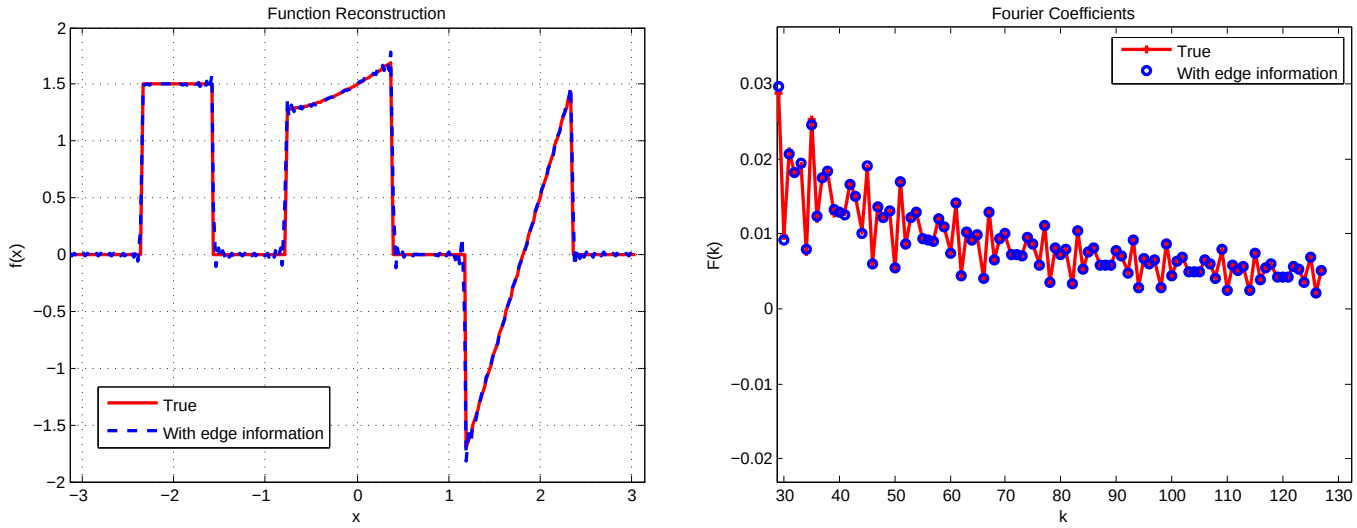

(a) Reconstruction - Using edge information

(b) The high modes - Using edge information

Figure: Reconstruction of a test function using edge information

Spectral reprojection for Fourier Frames (Gelb & Hines, 2010)

Finite frame approximation: Assume $\{e^{i\omega_n x}\}_{n\in\mathbb{Z}}$ is a frame for $L^2(I)$.

- Given frame coefficients $\{\hat{f}(\omega_n)\}_{n=-N}^{N} = \{< f(x), e^{i\omega_n x} >\}_{n=-N}^{N}$
- Compute $T_N f = \sum_{n=-N}^{N} \hat{f}(\omega_n) S^{-1} e^{i\omega_n x}$
- Filtering *does not* improve convergence:
  $T_N^{\sigma} f = \sum_{n=-N}^{N} \sigma(\omega_n)\hat{f}(\omega_n) S^{-1} e^{i\omega_n x} \nrightarrow f$
- Spectral reprojection yields exponential convergence.

Theorem (Gelb and Hines (2010)): Let $\{e^{i\omega_n x}\}_{n\in\mathbb{Z}}$ be a frame generated by a *balanced sampling sequence*. Suppose we are given the first $2N+1$ frame coefficients of $f \in L^2[-1,1]$. If $\lambda = \alpha N$ and $M = \beta N$ for $0 < \alpha < 1$ and $0 < \beta < 1$, then there exists a constant $0 < q < 1$ such that

$$||P_M^{\lambda}(f - T_N f)||_{\infty} \leq cN^2 q^N$$

Spectral reprojection for Fourier Frames (Gelb & Hines, 2010)

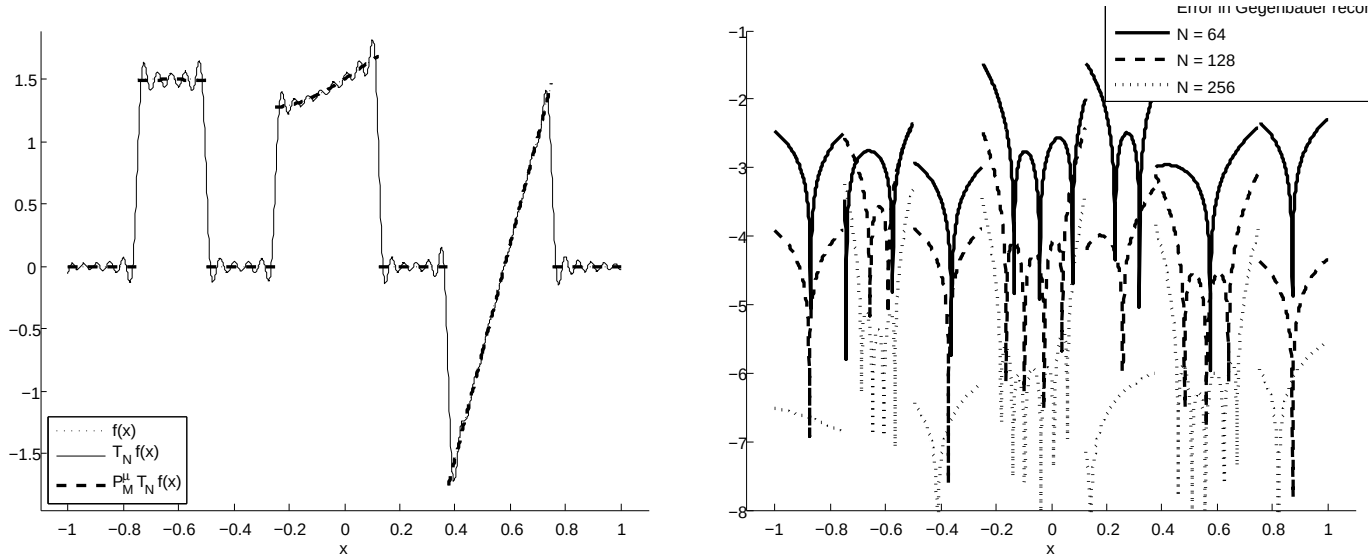

(a) Reconstruction with Gegenbauer frame algorithm

(b) pointwise error with Gegenbauer frame algorithm

Figure: Gegenbauer frame reconstruction

Spectral reprojection for Fourier Frames (Gelb & Hines, 2010)

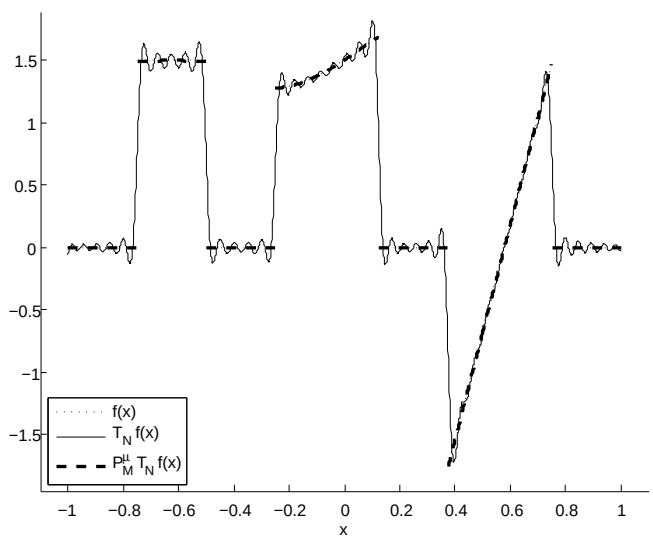

(a) Reconstruction with Gegenbauer frame algorithm

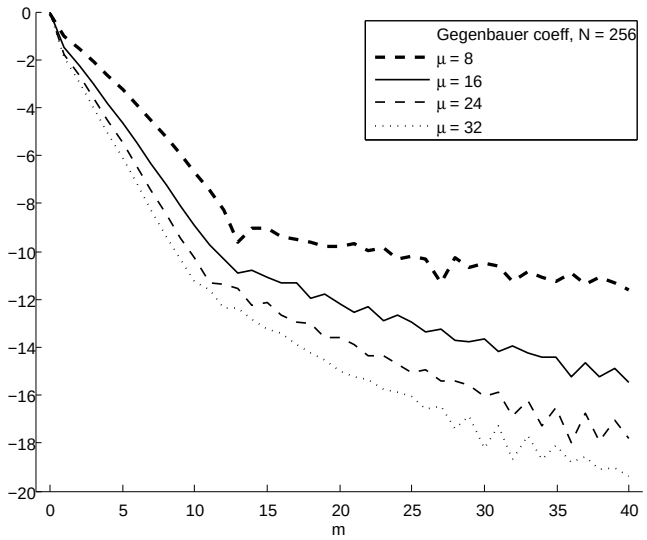

(b) coefficient decay

Figure: Gegenbauer frame reconstruction

Spectral reprojection for Fourier Frames (Gelb & Hines, 2010)

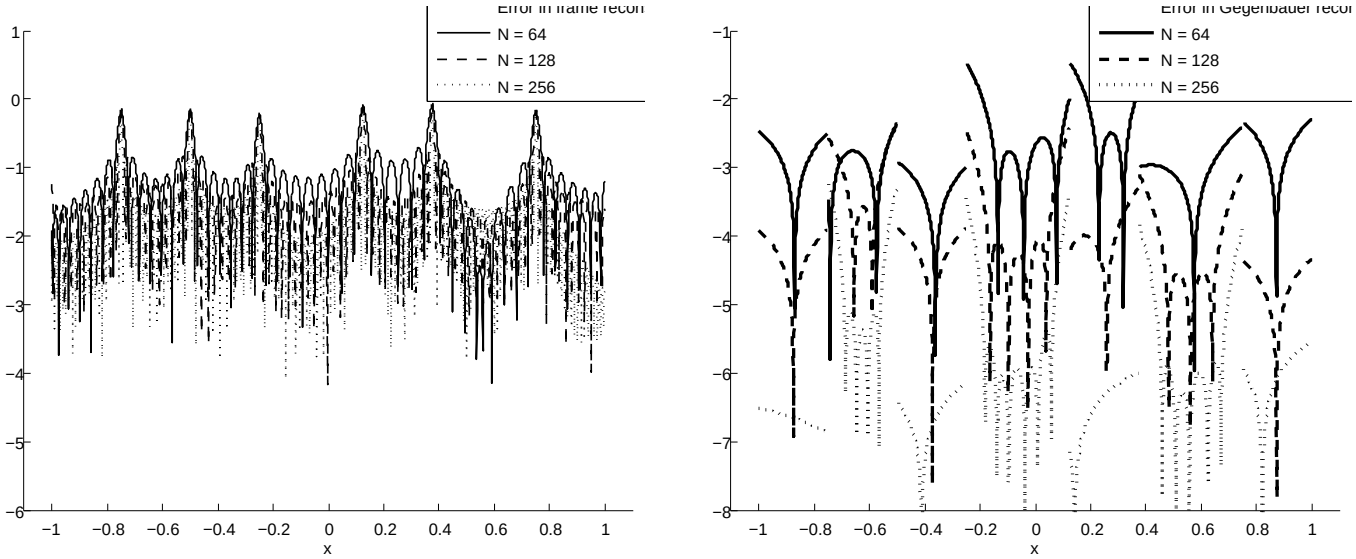

(a) pointwise error with frame reconstruction

(b) pointwise error with Gegenbauer frame algorithm

Figure: Gegenbauer frame reconstruction

Summary

- Problem: Fourier reconstruction of piecewise smooth functions from non-uniform coefficients – MRI, SAR
- Corresponding partial sum does not converge to underlying function
- Conventional reconstruction methods from MRI community (density compensation, uniform resampling, iterative methods)
- Error analysis and characteristics related to sampling density
- *Spectral reprojection* mitigates the impact of the error from the high frequency coefficients
- Fourier based edge information can help to obtain better approximation to high frequency coefficients
- Fourier frames may provide a better alternative in reconstruction since no interpolation is needed
- Special thanks to Adityavikram Viswanathan, ASU EE PhD 2010, currently a postdoctoral fellow at ACM. California Institute of Technology.

Problems we are working on

- Other interpolation schemes for Fourier data, for example radial basis functions. How do they fit into the general framework of approximation theory? Can we get better results for various sampling patterns? multiple dimensions?
- Approximation of the dual frame operator S^{-1}: Can we construct the finite operator $S_N^{-1} \rightarrow S^{-1}$? What is the rate of convergence and what is the numerical cost?
- Impact of noise on approximations and edge detection: Can we build a good statistical test bank to help distinguish edges from noise?
- General approximation theory: Rigorous analysis of our numerical methods' convergence rates, conditioning, and stability.
- Can we build more flexible frames that might be useful in function approximation?
- Possible applications to PDEs; imaging

Research Theme:

Consider a finite collection of data given as $\{(T_N[f](x))_j\}_{j=1}^N$, where f is bounded on $[a,b]^d$. How should we design a finite projection operator P_M such that $P_M(T_N[f])(x) \to g(f(x))$?

1. What restraints must be placed on the collected data, $\{(T_N[f](x))_j\}, j = 1, \cdots, N$, in order to construct a numerically stable operator P_M? What types of perturbations are tolerated?
2. In what sense does the approximation converge to $g(f(x))$?
3. Are the corresponding numerical algorithms viable, especially in multi-dimensions and as data size increases?
4. Are there preconditioning techniques that can improve numerical conditioning and efficiency without compromising accuracy?